5-20-2023

Behavioral Comparison of Fluorescent Tracer Sediment to Lightweight Polystyrene Sediment of the Lower Mississippi River Physical Model (LMRPM)

Julia C. Mudd
Louisiana State University and Agricultural and Mechanical College

BEHAVIORAL COMPARISON OF FLUORESCENT TRACER SEDIMENT TO LIGHTWEIGHT POLYSTYRENE SEDIMENT OF THE LOWER MISSISSIPPI RIVER PHYSICAL MODEL (LMRPM)

A Thesis

Submitted to the Graduate Faculty of the
Louisiana State University and
Agricultural and Mechanical College
in partial fulfillment of the
requirements for the degree of
Master of Science

in

The Department of Civil and Environmental Engineering

by
Julia Charlotte Mudd
B.S., Tulane University, 2017
August 2023

Acknowledgements

I would like to thank Dr. Zhiqiang Deng for his guidance on my thesis and for teaching me the foundation of water resources engineering and modeling. To Dr. Kory Konsoer who inspired the river scientist in me and helped me for hours with my experiments, MATLAB, and my data analysis. Thank you to The Water Institute and the CPRA for awarding me the grant to explore this idea. To all the graduate and undergraduate students at the LSU Center for River studies who both taught me everything I know about the Lower Mississippi River Physical Model, helped me for hours working on my flume experiments, and always kept my spirits high. To Mark Lee for bringing my flume dreams to fruition and making the Center for River Studies feel like home. I would like to thank my friends and family for their unwavering support; Colin Anderson, specifically, for being my Gandalf and teaching me how to be an adult, and my partner, Leon Sanford, for holding my hand through everything, reminding me to laugh, and making soul-sustaining curry to keep me going through it all. But most importantly, I would like to thank Dr. Clinton Willson, for all his reassuring advice, support, bad jokes, and for making me excited to learn again. I couldn't have asked for a better advisor to guide me through such a life-changing three years.

Table of Contents

List of Tables

List of Figures

Abstract

A lightweight, unexpanded polystyrene sediment with a specific gravity of 1.05 and a D10, D50 and D90 of 0.250 mm, 0.425mm, and 0.800 mm, respectively, is utilized in the Lower Mississippi River Physical Model (LMRPM) at Louisiana State University to mimic the sand transport of the Lower Mississippi River. While the black model sediment is easily visible against the stark white of the LMRPM, the relative homogeneity of the sediment particles and the opaqueness of the model channel make it difficult to closely study sediment dynamics during an experiment. For this reason, a tracer sediment that is marked with fluorescence and magnetic properties was tested to allow for more quantitative tracking of particles, and therefore an enhanced understanding of sediment transport and dynamics in the LMRPM. While these particles share similar density and relative grain sizes, parameters such as their angularity, settling velocities, and threshold for incipient motion are unknown. Angle of repose, settling velocity, and incipient motion tests are conducted to estimate these parameters and compare the tracer sediment behavior to that of the model sediment to determine how the tracer sediment can eventually be employed in the LMRPM. While differences do exist between the sediments' settling velocities and angles of repose, incipient motion tests that combine the two sediments reveal surprisingly similar thresholds for motion, suggesting that the tracer sediment can be implemented in the LMRPM to study punctuated sand transport and the evolution of sand bars around sediment diversions. A pilot study where tracer sediment was seeded in the sand bars upstream of the Mid-Breton and Mid-Barataria Sediment Diversions produced positive results, bolstering the use of the tracer sediment in the LMRPM.

Chapter 1. Introduction

1.1. Overview and Objectives

The Louisiana State University's Center for River Studies in Baton Rouge, Louisiana houses a 10,000 square foot, mobile-bed, physical model of the Lower Mississippi River from Donaldsonville to the Bird's Foot Delta in the Gulf of Mexico (Figure 1). The Louisiana Coastal Protection and Restoration Authority (CPRA) constructed this model to study the dynamic riverine and bedload processes occurring along the lower river and how these processes are affected by proposed diversion projects. The model is scaled horizontally 1:6000 and vertically 1:400, creating a distortion ratio of 15, to fit space constraints while maintaining appropriate Reynold's numbers (CPRA, 2019).

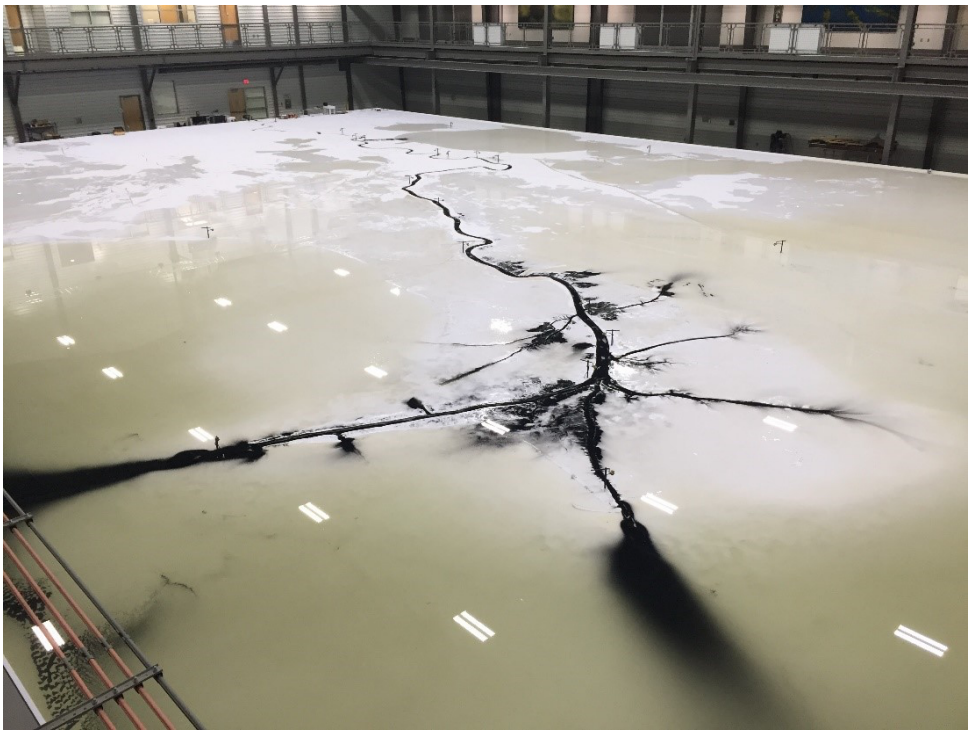

Figure 1. View of the LMRPM.

Model flows are scaled based on Froude similitude with the prototype. A lightweight, unexpanded polystyrene sediment with specific gravity of 1.05 was chosen to mimic the sand in the real Mississippi River (Figure 3). The sediment size is scaled based on the similitude of the critical Shields parameter and the critical particle Reynolds number, resulting in the model sediment having diameters 3.2 times the prototype sediment diameters. Because both parameter ratios are scaled at their critical values, the model and prototype sediment have the same threshold for initiation of motion (Hooper, 2019). From extensive scaled flume experiments conducted by Hooper (2019), it was found that dune heights and lengths were similar to those found in the replicated reaches of the Mississippi River. By adjusting the sediment time scale to 6600, model sediment morphodynamics most closely resembled those of the prototype and made one hydrographic year on the Mississippi River executable within approximately one hour in the model (Hooper, 2019).

At the LMRPM, "50-Year" experiments are conducted to test the effects of relative sea level rise and sediment diversions on the hydraulics and bulk sand transport in the Lower Mississippi River. Historical hydrographs from 1964 to 2013 and an incremental relative sea-level rise of 2.3 ft are used for the 50 year experiments to determine how bed levels and river stages are impacted by sediment diversions as compared to the "50-Year Future without Action" scenario that depicts the lower river 50 years into the future without any sediment diversion or other land-building projects. Each 50-Year experiment is completed twice to test for replicability. So far, 50 years with the Mid-Barataria Sediment Diversion (Figure 2) and 50 Years with the Mid-Breton Sediment Diversion have been completed, and 50 Years with the Combined operation of the Mid-Barataria and Mid-Breton Sediment Diversions are currently being conducted. The stage and sediment bed elevation data that are collected from these experiments provide valuable

quantitative evidence of the effects that the diversions and relative sea level rise may have on the river stages and sediment transport processes up and downstream of the diversions. However, research on the qualitative aspects of the bulk sand transport around the model's diversions during a given hydrographic year is lacking.

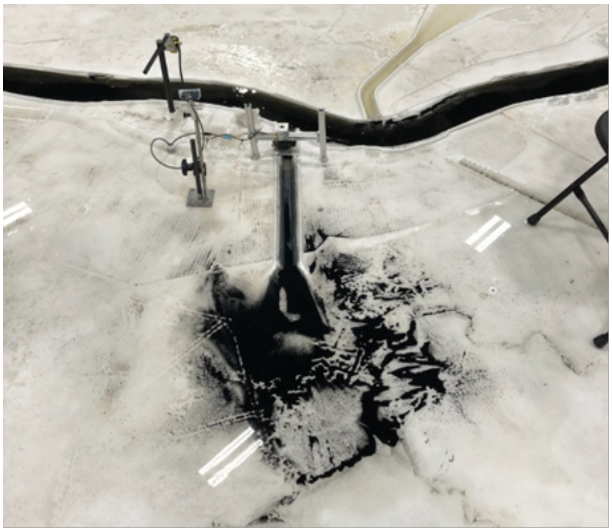

Figure 2. Mid-Barataria Sediment Diversion on LMRPM.

Of particular interest at the LMRPM is the punctuated sand transport phenomena (Nittrouer et al., 2011) and the evolution of sand bars along the river and near sediment diversions (Yuill et al., 2016). The study of this phenomena is rather difficult with an opaque channel and a homogenous black sediment. For this reason, a green, fluorescent, and magnetic sediment with specific gravity of 1.05 and average particle diameter of 0.425 mm was purchased from Metaflake to be employed in LMRPM experiments with a goal of improved visualization and quantification of bedload transport. The fluorescence allows for the tracer particles to be easily differentiated from the existing sediment, and the magnetism allows for a simpler way to collect and measure the tracer volumes. By injecting a certain mix of the tracer and model sediment into the model

once every 5 model years, or seeding sand bars along the river, the implementation of a tracer creates opportunities for in-depth, site specific studies on sand transport in the LMRPM.

Before the tracer sediment is implemented in the model, several sediment analyses need to be conducted to ensure the tracer particles behave similarly to the model sediment already in use. To understand the durability of the tracer particles, samples were exposed to chlorine, detergent, and agitation that model sediment particles are exposed to daily, and observations as well as sieve analysis were conducted every 5 days over a 15-day sampling period. Water displacement tests were conducted to compare the density and porosity of the tracer to that of the model sediment. Then, settling velocities were measured for different grain size classes and compared to their theoretical values. Angle of repose tests were conducted to compare the angularities of the sediments. Finally, incipient motion tests were conducted in a hydraulic flume to compare the shear stress thresholds needed for motion for model and tracer sediments.

1.2. Literature Review

1.2.1. Sediment Analysis

Many different types of non-cohesive sediment have been experimented with in physical river models with mobile beds – from low density particles such as ground walnut shells and polystyrenes, to typical high density sand mixtures- all to recreate sediment dynamics at varying scales (Kleinhans et al., 2017). When working with scaled models, various sediment types can be considered to accurately mimic prototype sediment transport as long as similitude exists between the model and prototype sediments' Shields parameter and Reynold's particle number (Ho et al., 2010; Julien & Tuzson, 2003; Pugh & Dodge, 1991). The black, lightweight, unexpanded polystyrene sediment utilized in the LMRPM was chosen to best mimic the transport of Mississippi

River sand once the diameters were scaled to meet the critical Shields parameter and critical Reynold's particle number criterion (Hooper, 2019).

The scaling of these diameters was done by first setting the ratios of both the critical particle Reynold's number, Re_{c*}, and the critical Shields parameters, τ_{*c}, to unity. Then, the following derivation was used to scale the diameters of the prototype, d_p, to the model, d_m (BCG Engineering & Consulting, 2015):

$$(Re_{c*})_p = \frac{d_p(u_{*c})_p}{v}$$

$$(Re_{c*})_m = \frac{d_m(u_{*c})_m}{v}$$

$$(Re_{c*})_p = (Re_{c*})_m$$

$$\frac{(u_{*c})_p}{(u_{*c})_m} = \frac{d_p}{d_m} \qquad \text{Eq. 1.10}$$

$$(\tau_{*c})_p = \frac{(u_{*c})_p{}^2}{g(G_p - 1)d_p}$$

$$(\tau_{*c})_m = \frac{(u_{*c})_m{}^2}{g(G_m - 1)d_m}$$

$$(\tau_{*c})_p = (\tau_{*c})_m$$

$$\frac{(u_{*c})_p{}^2}{(u_{*c})_m{}^2} = \frac{g(G_p-1)d_p}{g(G_m-1)d_m}\ , \qquad \text{Eq 1.11}$$

where v is the kinematic viscosity of water, u_{*c} is the critical shear velocity, g is gravitational acceleration, and G_p and G_m are the specific gravities of the prototype and model sediments, respectively. After combining Equation 1.10 and Equation 1.11, a relationship between model sediment diameter and prototype sediment diameter results:

$$d_m = d_p[(G-1)_r]^{1/3} \qquad \text{Eq. 1.12}$$

The model sediment is a ground, unexpanded polystyrene with a density of 1.05 g/cm^3 (Figure 3), compared to the prototype river sand made of silica from quartz that has a density of 2.65 g/cm^3. After substituting in the specific gravity, G, of the model and river sediment into Equation 1.12, the final ratio between model and prototype sediment is:

$$d_m = 3.2 d_p \qquad \text{Eq. 1.13}$$

The resultant grain size distribution of the model sediment in Table 1 is based on this ratio as well as the grain size distribution of Mississippi River sand retrieved from a survey in the region below New Orleans (BCG Engineering & Consulting, 2015):

Table 1. D10, D50, and D90 grain sizes in millimeters for sand from Prototype River (Mississippi River) and the resultant scaled sediment for the LMRPM.

Sediment Type	D10 (mm)	D50 (mm)	D90 (mm)
Prototype (Mississippi River Sand)	0.08	0.12-0.14	0.25
Model (LMRPM)	0.25	0.40-0.45	0.80

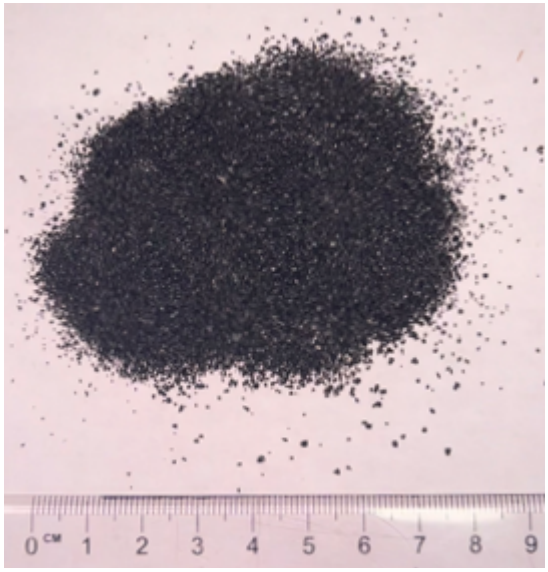

Figure 3. Black, lightweight, unexpanded polystyrene sediment used in the LMRPM. Grain sizes range from 0.1mm to 1.0mm.

By finding the velocity thresholds for incipient motion, the critical Shields parameter of a sediment can be estimated. Incipient motion, or the very beginning of movement for sediment particles, is achieved when flows introduce just enough shear stress to the bed to overcome the gravitational and frictional resistive forces of the sediment particles, causing the particles to begin to roll, slide, and saltate (Vollmer & Kleinhans, 2007). The near-bed turbulent fluctuations that initiate this motion can then be used to calculate shear stresses at the bed and the resultant Shield's parameter, which is an important indicator for sediment transport behavior (Hooper, 2019). Therefore, comparing different sediments by their incipient motion thresholds can be a useful mechanism in determining whether they will behave similarly under the same hydraulic conditions.

Critical thresholds for sediment motion have been a topic of much debate amongst specialists due to their subjectivity and the many different methods of estimating them. Kramer (1935) separated observations of sediment movement into four categories that entailed "zero transport" or no motion of particles, "weak transport" or a few small particles moving in specific isolated

locations, “medium transport” or several grains of a mean diameter moving in a small discharge, and “general transport” or grains of all sizes moving constantly all across the bed surface (Kramer, 1935; Lavelle & Mofjeld, 1987). Even then, he discussed the difficulty of separating observations into these categories, as many observations seemed to display characteristics of more than one category. Regardless, Kramer considered the critical stress threshold to be that which caused general transport. Vanoni (1964) on the other hand, considered Kramer’s definition of weak transport to line up with Shields’ definition of incipient motion. He also considered the critical stress threshold to be when particle motion occurs at least every 2 seconds anywhere on the bed surface (Vanoni, 1964), while also noting there is no stress below which not even minor particle motion will occur (Vanoni et al., 1966). Because particle motion can occur due to random fluctuations in instantaneous bed shear stress in hydraulically smooth, transitional, and turbulent flow regimes (Grass, 1970), Lavelle and Mofjeld (1987) argue that a critical threshold for particle motion does not exist and should not be of importance when studying quantitative sediment transport. Rather, the focus should be on erosion rates (Lavelle & Mofjeld, 1987). However, for this study, comparing thresholds of motion between two sediments is a useful way to determine how similarly they will behave in the same hydraulic settings.

Shields (1936) developed a set of equations that plotted a single curve representing the “critical tractive force” on angular grains of uniform size. This curve, also termed as the Shields diagram (Figure 4), paved the way for future incipient motion studies, and was used to estimate the critical tractive force for both the LMRPM model sediment and the tracer sediment obtained for this study. Theoretically, particle motion should occur at any tractive force above the Shields curve for a given sediment of a certain size and density.

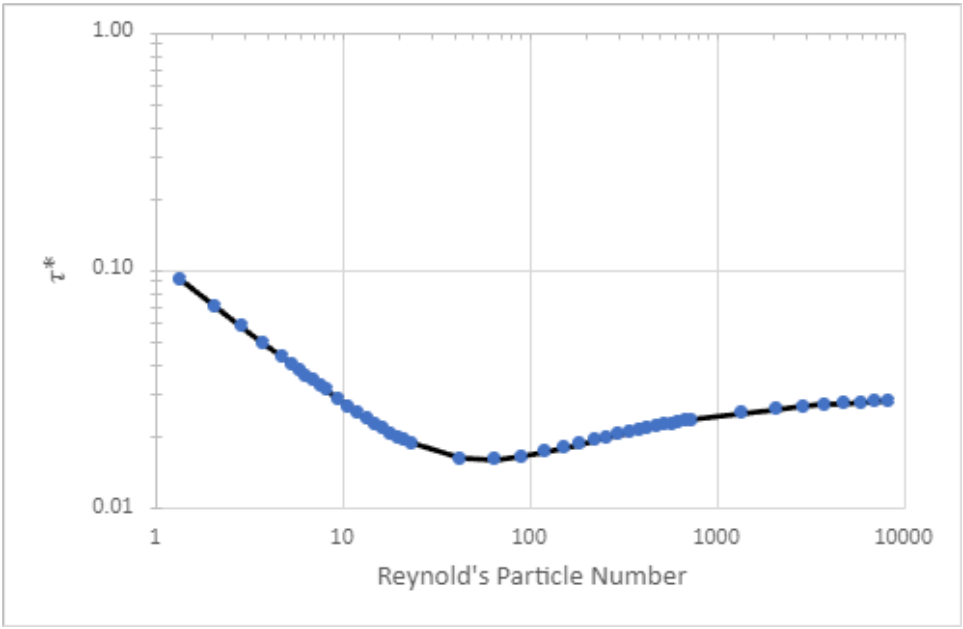

Figure 4. Shields Diagram showing Reynold's Particle number at water temperature of 21.1° C with sediment SG 1.05 and varying sediment diameters from 0.15mm to 50mm versus the dimensionless Shields Parameter, τ*, representing critical tractive force for initiation of sediment motion. Shields parameters and Reynold's particle numbers calculated using equations from Parker et al. (2003).

Shields noted that observations of incipient motion are more accurate when the sediment size is more uniform, or well-sorted, and the sediment bed is smoother (Shields, 1936). He and other specialists such as Grass (1970) noted that incipient motion is more dependent on probabilistic functions centered around bed shear stress and the shapes, sorting, and packing of the bed material (Buffington & Montgomery, 1997). Other specialists, such as Wiberg and Smith (1987) created new equations to account for sediment mixtures with varying grain sizes, noting that the particle angle of repose changes with mixtures and that this will dramatically change the critical shear stress estimates for such sediment. This is due to the increased drag force acting on coarser grains that protrude farther into the flow than finer grains (Einstein, 1950). Meanwhile, finer grains tend to nestle in between coarser grains and are not exposed to the same amount of drag force, a phenomenon caused by the so-called "hiding effects" (Einstein, 1950). Even though the coarser grains normally require more shear stress to initiate motion compared to finer grains, when in more poorly-sorted mixtures, the difference in shear stress to incite motion for coarse and

fine grains is reduced. Therefore, depending on the sorting of the mixture, the observed threshold for incipient motion of particles in a mixture might not be as dramatically different from the theoretical threshold for motion (Einstein, 1950; Wiberg & Smith, 1987).

Other important parameters of a sediment that affect its transport include the particle's density, size, shape, angle of repose, and settling velocity. Both the particle density and grain size are essential variables in equations for the Reynold's particle number, the critical Shields parameter and dimensionless (Shields) shear stress, τ_c* and τ*, respectively, and the theoretical settling velocity. Settling velocity can indicate a sediments propensity to fall out of suspension due to changing flows, which can affect spatial and temporal deposition trends (Pugh & Dodge, 1991). The shape and size of the grains are the key variables that affect a sediment's angle of repose (Julien & Tuzson, 2003), which act as a measure of interparticle friction and can signify the degree of resistance to motion of a particle when resting on a bed surface amongst other similar particles (Wiberg & Smith, 1987). The angle of repose is thus relevant to incipient motion of sediment particles and subsequent dune formation and migration. When analyzing the current model sediment for use in the LMRPM, Hooper, for BCG Engineering & Consulting, Inc. (2015), conducted several tests to calculate its density, angle of repose, and settling velocities and compare it to other potential sediments for use in the model. These tests are therefore replicated in this thesis to provide a full analysis of the tracer sediment and a direct comparison to the model sediment.

1.2.2. Sediment Transport Trends in Lower Mississippi River

Flow in the Lower Mississippi River (miles 0-400, river kilometers 0-650) is considered nonuniform, as this segment experiences significant backwater effects due to the reduction in water surface slope as the river approaches the Gulf of Mexico (Nittrouer et al, 2012). These backwater effects reduce the skin friction shear stress acting on the sand in the bed to just below the critical

value necessary to suspend the sand and transport it down river during low to moderate discharges. Conversely, during high discharges, shear stress is increased almost 10-fold and suspends sand from the bed to transport it downstream. These hydrodynamic characteristics have been termed "punctuated" sediment transport or "pulse-like" dynamics (Nittrouer et al., 2011). Simultaneously, the Lower Mississippi River is unable to migrate laterally due to revetments that prevent the banks from eroding and supplying more sediment locally. Instead, high flows can scour the bed, exposing the substrate in bends and depositing sand downstream. The minimal bed load transport that occurs during low to moderate discharges is not sufficient to cover this substrate with sediment, as high discharges continue to deplete any local accumulation. Because of these dynamics, the beds of the Lower Mississippi River backwater segment and the LMRPM exhibit a "patchy"-like appearance; areas with exposed substrate are followed by straight reaches with significant accumulations of sediment (Nittrouer et al., 2012).

Studies on punctuated sediment transport in the LMRPM have yet to be conducted, presenting a need for an in-depth tracer study. While tracer sediments have been employed in the Mississippi River to study dynamics and deposition through sediment diversions (Allison et al., 2017), none have been employed in such a large-scale physical model of the river. The fluorescent and magnetic tracer sediment obtained from Metaflake will allow for a highlighted view of bedload sediment transport in the Lower Mississippi River Physical Model. The fluorescence will allow for specific particles to be differentiated from the homogenous black model sediment, improving the observations of localized sediment transport around river bends, up-and-downstream of sediment diversions, and in the Bird's Foot Delta. Meanwhile, the tracer's magnetism will facilitate the separation of the tracer from the model sediment during sediment sampling and dredging operations, to further quantify patterns of sediment transport. The use of this tracer

sediment in the LMRPM presents a myriad of opportunities for further research in sediment transport phenomena in physical models and the Mississippi River itself.

Chapter 2. Methodology

A fluorescent and magnetic tracer sediment was obtained with the intent of injecting it into the LMRPM alongside model sediment to further study sediment transport dynamics. The objective of this study is to directly compare the physical characteristics and behaviors of the tracer and model sediments to see if the tracer behaves similarly enough to the model sediment so that it can be used without impacting experimental data or results on the LMRPM. Comparisons of porosity, density, settling velocity, angle of repose, and Shields parameters provide a good understanding of any physical and behavioral differences between the particles. The results of these experiments will inform whether the tracer sediment will be able to accurately mimic the movement of the model sediment and therefore be employed in the LMRPM. Ultimately, a pilot experiment involving the seeding of the sand bars upstream of the Mid-Breton and Mid-Barataria sediment diversions in the LMRPM with tracer sediment was conducted and provided a glimpse of how the tracer will move in the LMRPM with model sediment, while also helping to establish best practices for implementation and analysis of the tracer in the model for future experiments.

2.1. Chemicals and Agitation Exposure Tests

While the LMRPM model sediment is comprised of a black, unexpanded polystyrene material, the tracer sediment is comprised of polystyrene particles coated in a fluorescent and magnetic paint. The LMRPM model sediment has been utilized in experiments for 5+ years and has not shown signs of leaching its color or fining its particle sizes significantly over time. To ensure the tracer sediment will not leach its coating and/or break down over time during experiments on the model, the particles were tested to see how they react to the conditions they will be exposed to on the LMRPM. These conditions include agitation and constant inundation in water that contains chlorine bleach and liquid detergent. Every 100 gallons (378 liters) of water

injected into the LMRPM is mixed with about 200mL of Tide laundry detergent and 15mL of chlorine pool shock to both reduce the surface tension of the water with the model sediment and prevent bacterial and algal growth in the model. Exposure tests will reveal if the tracer sediment coating begins to leach into the water, and/or if particles begin to breakdown, reducing grain sizes over time.

To conduct this experiment, five plastic, 2-liter buckets were set up as follows: 1) Control- 1.5L water; 2) Control- 1.5L water, 2mL tide, <1ml chlorine; 3) 500ml tracer sediment, 2mL tide, 1L water; 4) 500ml tracer sediment, 2mL tide, <1ml chlorine, 1L water; 5) 500ml tracer sediment, 2mL tide, <1ml chlorine, 1L water, agitated 2hrs/day. Observations and sediment samples were taken every 5 days over a 15-day sampling period.

The sediment used in the buckets was taken from the original batch of tracer sediment, and this "original" sediment was sampled every 5 days as well for comparison. For the agitated sample, a motorized mixing station, comprised of a hand drill connected to an adjustable motor, was set up to agitate the sample 2 hours daily. Daily videos were taken to document the overall appearance of the mixtures and look for any possible leaching of tracer coating into the water or rusting of the particles. On day zero and the fifth, tenth, and fifteenth days of the experiment, about 75 grams of sediment were sampled from each of the buckets containing sediment and set out to dry. Once completely dry, samples were analyzed by sieves to obtain sediment size gradations to see if particles had broken down or fined due to loss of coating over the sampling period.

2.2. Porosity and Density Tests

While the tracer sediment was specified to have the same density as the model sediment, this parameter needed to be tested and confirmed. Density of the particles is a crucial parameter affecting sediment transport, and thus necessary in the equations for determination of the critical

Shield's parameter for incipient motion. Porosity and density tests were conducted for both the model and tracer sediments for comparison.

Following the work done by Hooper (BCG Engineering & Consulting, 2015), a 100ml graduated cylinder is weighed and the weight is recorded. The cylinder is then filled with 25mL of sediment, the sediment is compacted, and then the cylinder with sediment is weighed and recorded. A separate 100mL graduated cylinder is filled with 25mL of water. The 25mL of water is slowly poured into the graduated cylinder with the sediment, allowing for the water to infill the void spaces of the sediment. The new volume in the graduated cylinder is recorded. This procedure is repeated two more times and then again for a sediment volume of 50mL with a corresponding water volume of 40mL, to test for consistency of porosity and particle density values. This process is completed for both the model and tracer sediments.

The porosity is then calculated by the following equation:

$$Porosity = \frac{V_{sed}+V_{water}-V_{sed+water}}{V_{sed}} * \ 100\%, \qquad \text{Eq. 2.10}$$

where V_{sed} is the volume of the dry, compacted sediment, V_{water} is the volume of the water before it is added to the sediment and $V_{sed+water}$ is the volume of the combined water and sediment. The particle density is calculated by the following equation:

$$Particle\ Density = \frac{W_{sed}}{V_{sed+water}-V_{water}}, \qquad \text{Eq. 2.11}$$

where W_{sed} is the weight (g) of the dry, compacted sediment.

2.3. Settling Velocity Tests

Due to the tracer particles' differing shape, coating, and density, the tracer particles may settle at different rates than the model sediment. Settling velocities of the model and tracer

sediment are measured following the tests outlined by Hooper (BCG Engineering & Consulting, 2015), and compared to calculated theoretical settling velocities.

The sediments are sieved into three different grain size classes: 0.850-0.500mm (sieve size No. 20 and 35), 0.500-0.355mm (sieve size No. 35 and 45), and 0.355-0.150mm (sieve size No. 45 and 100). Each grain size class is placed in its own cup and mixed with water and <1mL of liquid detergent to reduce surface tension. A 4000 mL graduated cylinder is filled with water and a "starting mark", labeled "0", is measured to be 18.2cm below the water fill line to allow for particles to reach a uniform settling velocity. A 50mm, 100mm, and 200mm mark were measured below the starting mark, as seen in Figure 5. The water in the graduated cylinder is left to settle for 5 minutes to reduce disturbance in the water column that could impact settling velocities of particles, and then the water temperature is recorded. A spoonful of sediment is gently placed at the water surface and the sediment is dropped into the water column. The timer is started when the bulk of particles reaches the "0" mark and stopped at the 50mm mark for the 0.355-0.150mm particles. The time is recorded and then this procedure is repeated five times, before moving onto the next grain size class. The 0.500-0.355mm particles are timed over the 100mm distance and the 0.850-0.500mm particles are timed over the 200mm distance.

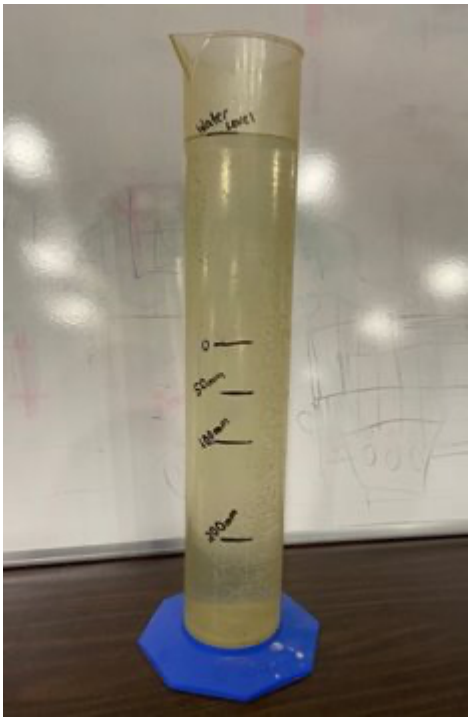

Figure 5. 4000mL graduated cylinder used in settling velocity tests.

Measured results are then compared to theoretical values calculated from both Pierre Julien's (Eq. 2.12) (Julien & Tuzson, 2003) and Gabriel Stokes' (Eq. 2.13) (Stokes, 1901) equations for settling velocity:

$$\omega_0 = \frac{8v}{d_s}\left\{\left[1 + \frac{(G-1)g}{72v^2} d_s^3\right]^{0.5} - 1\right\} \qquad \text{Eq. 2.12}$$

$$\omega_0 = \frac{1}{18}\frac{(G-1)g}{v} d_s^2 \,, \qquad \text{Eq. 2.13}$$

where ω_0 is the settling velocity of a sediment particle in clear water, G is the specific gravity of the sediment, υ is the kinematic viscosity of water, and d_s is the sediment particle diameter. The main difference between these two equations is that Stokes' Law is specifically for spherical grains. These equations are valid under the assumption that flow in the water column is laminar, i.e., the Reynold's number is less than 1. Reynold's numbers are calculated using:

$$Re = \frac{ud_s}{v}, \qquad \text{Eq. 2.14}$$

where u is the observed settling velocity of a particle of size d_s.

2.4. Angle of Repose Tests

The angle of repose of a sediment is affected by the surface area, shape, and density of the particles (Al-Hashemi & Al-Amoudi, 2018). While the densities between the tracer and model sediments are similar, the tracer particles are spherical, whereas the model sediment particles are highly angular. High resolution photographs were taken with a microscope to show the differences between particles (Figure 6 and Figure 7).

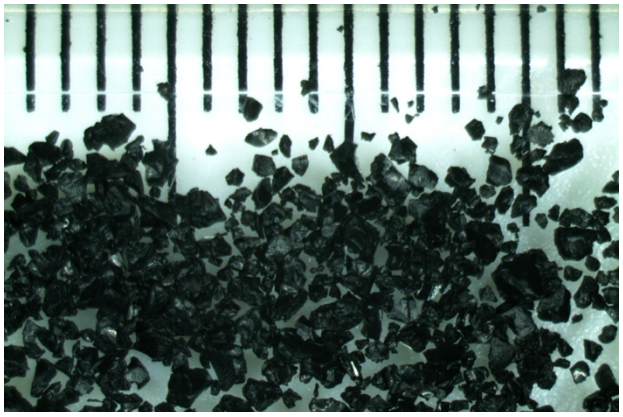

Figure 6. Photo of unexpanded polystyrene sediment used in LMRPM, taken with a microscope

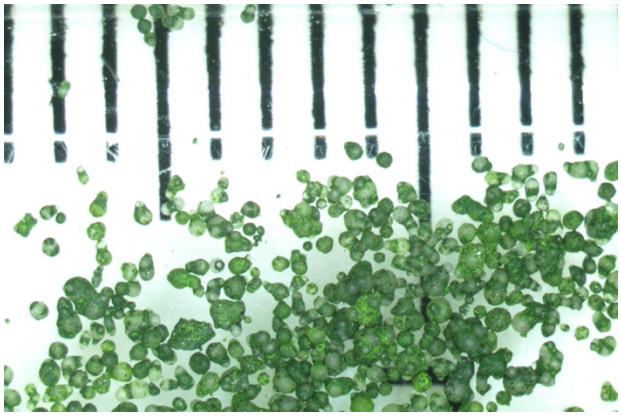

Figure 7. Photo of polystyrene magnetic and fluorescent tracer sediment from Metaflake taken with a microscope

The angularity of the sediment particles will affect bed load transport and dune and other bedform geometries, so a comparison of each sediment's angle of repose is necessary. To measure each sediment's angle of repose, a cylindrical glass mason jar is filled halfway with saturated

sediment and halfway with water. The jar is sealed tightly with a lid, shaken, and then placed on its side atop two PVC tubes that are taped horizontally to a flat surface (Figure 8). Once the sediment settles for 15 minutes, a protractor is held so the zero degree line is lined up with the horizontal surface of the sediment. The jar is rotated slowly, while maintaining the position of the protractor, until sediment particles begin to roll down the slope or sink on one side. The angle on the protractor that corresponds to the sediment surface when movement begins to occur is recorded. This procedure is repeated 5 more times, and an average angle of repose is calculated. This experiment is conducted on four different mixtures of sediment: 1) a batch of the Model sediment full grain size range with D10=0.35mm, D50=0.52mm, and D90=0.83mm, 2) Model Sediment D50 grain size range with D10=0.33mm, D50=0.44mm, D90=0.56mm, 3) Tracer sediment D50 grain size range with D10=0.32mm, D50=0.44mm, and D90=0.56mm, and 4) Tracer and model mix, with the tracer replacing the D50 grain size of the model sediment full grain size range, D10=0.21mm, D50=0.44mm, D90=0.79mm.

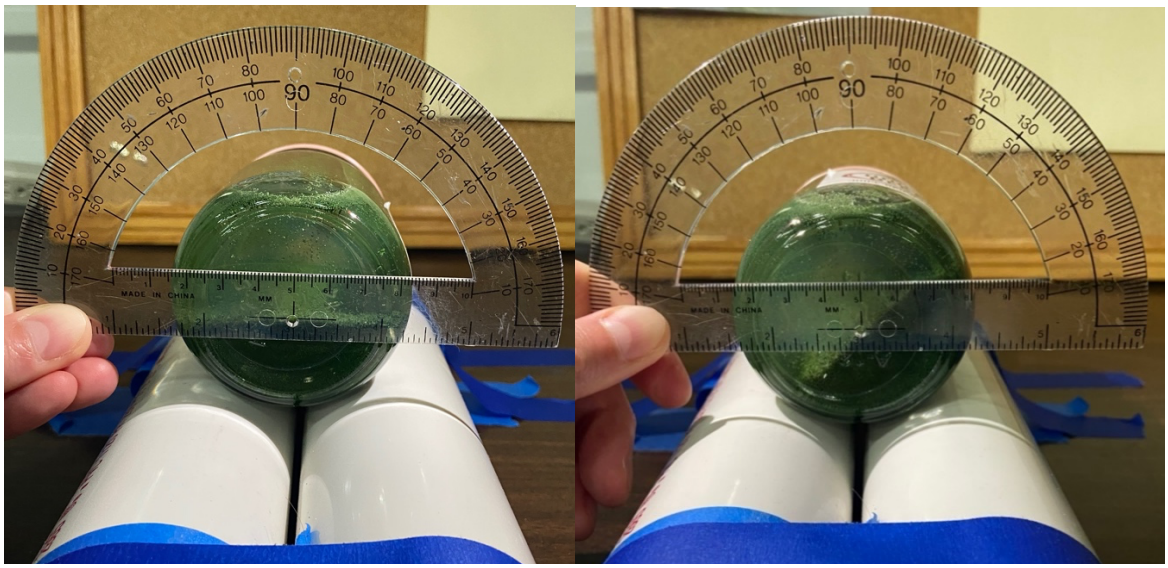

Figure 8. Mason jar filled with tracer sediment and water. Left: Starting position for angle of repose tests. Right: mason jar being rotated to find angle of repose.

2.5. Incipient Motion Tests

The LMRPM sediment diameters were scaled based on the particle Reynold's number and critical Shields parameter similitude with the prototype (Mississippi River sand), meaning the model and prototype sand share the same threshold for incipient motion. Therefore, the similarity of velocities and subsequent shear stresses needed to initiate particle movement between the model sediment and the tracer sediment are a good indicator of whether the sediments will behave similarly under varying flow conditions. If the sediments share similar critical Shields parameters, the tracer sediment could be implemented in the LMRPM alongside the model sediment in future experiments.

The objective of this experiment is to measure water velocities in a hydraulic flume that initiate sediment movement and then convert these recorded velocities to shear stresses to calculate the critical Shield's parameter for the model and tracer sediments. The thresholds for incipient motion of the model sediment are then compared to those of the tracer sediment.

Four series of flume tests are conducted to test incipient motion of sediment particles. A 4-meter-long flume (Figure 9) with 3.5 m working length was designed and built to mimic the 5-meter long Armfield S6 AKII flume used in the experiments done by Hooper (2019). The LMRPM hydraulic flume is made out of clear, cast acrylic and has two channels, each 0.13 meters wide to mimic the LMRPM river channel width. Upstream and downstream weirs, each with a height of 8 cm, were installed in one channel to maintain a water depth of at least 6cm over the bed to mimic average LMRPM water depths. An EVENTEK KPS3010D DC Power Supply (0-30V, 0-10A) was used to power a Rule 2000 Bilge Pump that fed water from the upstream reservoir tank through a Blue-White Industries, Ltd. F-2000 Flow Meter and up into the flume.

A 16 MHz Sontek MicroADV (acoustic Doppler velocimeter) is used to measure instantaneous three-dimensional water velocities (30 Hz sampling frequency) near the sediment bed. Mean velocities and their fluctuations in the x, y, and z directions are then used to calculate turbulent kinetic energy (TKE), bed shear stresses, and resultant critical shear stress for particle motion. The first flume test is a replication of the test described in Hooper (2019) using the full range of sizes of the model sediment of the LMRPM. The flume is then cleaned, and the experiment is repeated 3 more times using: 1) the D50 of the LMRPM model sediment (0.355-0.500 mm); 2) tracer sediment particles that are of the same size as the LMRPM D50 (0.355-0.500 mm); 3) the full range of particles of the LMRPM model sediment with the D50 size fraction replaced by the 0.355-0.500 mm tracer particles.

For the experiment set up, 9 circular plastic tubes of 4 cm diameter and 15 cm length are taped together and inserted in the hydraulic flume just downstream of the upstream weir to help align the flow. The flume is filled with water, achieving approximately 9 cm depth. At about 1 m downstream of the upstream weir, a 1.5 m long, 2 cm thick layer of sediment is placed covering the channel bed and then screeded flat. This leaves a working depth of at least 7 cm of water above the 2 cm of sediment.

The MicroADV is positioned 2.25 m downstream of the first weir (Figure 10), at about 1.25 m of the 1.5 m working length of sediment. The bottom of the probe rests about 6.5 cm above the surface of the sediment bed to record velocities in the 0.5-1.5 cm region above the bed, as the ADV records point measurements at a minimum distance of 5 cm from the probes. The probe is then leveled horizontally and vertically.

Before each experiment (except Model Full Range Trials 1-4), a simple bucket test is run to calculate a relationship between an observed gallon per minute (GPM) flow rate to the flow rate

displayed on the flow meter. The bucket test is done by simply recording the amount of time it takes to fill 2 gallons in a bucket at varying pump voltages and then comparing these calculated GPMs to the observed flow meter GPMs. Additionally, before each trial of each experiment, the sediment bed is "fluffed", i.e., the surface of the sediment bed is disturbed lightly to ensure that settling occurring overnight will not affect particle motion at the bed surface. When the sediment has settled, the pump is started and gradually increased to a starting voltage of 5.8 (which corresponds to a flow of about 7 GPM or 4.42 E-4 m^3/s) for the model sediments and 4.6 (about 2.2 GPM or 1.39E-4 m^3/s) for the tracer sediments. The voltage is held constant for about 4 minutes to allow the flow to stabilize and ensure the flow has fully developed throughout the whole flume. Baby powder is added to the water by the upstream weir to add particulates to the water column so that the ADV signals are clearer. The correlation percentage and Signal to Noise Ratio (SnR) are checked throughout the experiment to make sure that they are reading close to 100% and above 20 decibels, respectively, to ensure that the ADV is receiving good readings (Sontek, 2001). Then, 90 seconds of ADV measurements are recorded simultaneously with video of the bed from upstream to downstream by the ADV. All observations are recorded.

The pump voltage is continuously increased by 0.2 volt increments and maintained for 4 minutes with simultaneous ADV and video recordings for each condition. Voltage increments may be decreased to find the most accurate velocity at which particles first begin movement. Any movement or sediment formations (dunes and scour holes) are noted throughout the experiment, along with the times at which they begin to occur. Once incipient motion is determined to be observed, a velocity profile is recorded. This is done by maintaining the pump voltage and positioning the ADV at probe heights 8 cm, 8.5 cm, 9 cm, and 9.5 cm above the flume bottom to record 90-second velocity measurements at 1 cm, 1.5 cm, 2 cm, and 2.5 cm above the sediment

bed, respectively. Afterward, the ADV is returned to its original elevation above the bed, and voltage is continuously increased until flows corresponding with general motion of sediment have been measured and recorded by the ADV. At the end of the experiment, another bucket test is conducted to ensure that the relationship between pump voltage and flow rate was consistent throughout the experiment. Finally, the flume is cleaned, and the experiment is repeated two more times, totaling 3 trials. This procedure is repeated for the 3 other scenarios listed above.

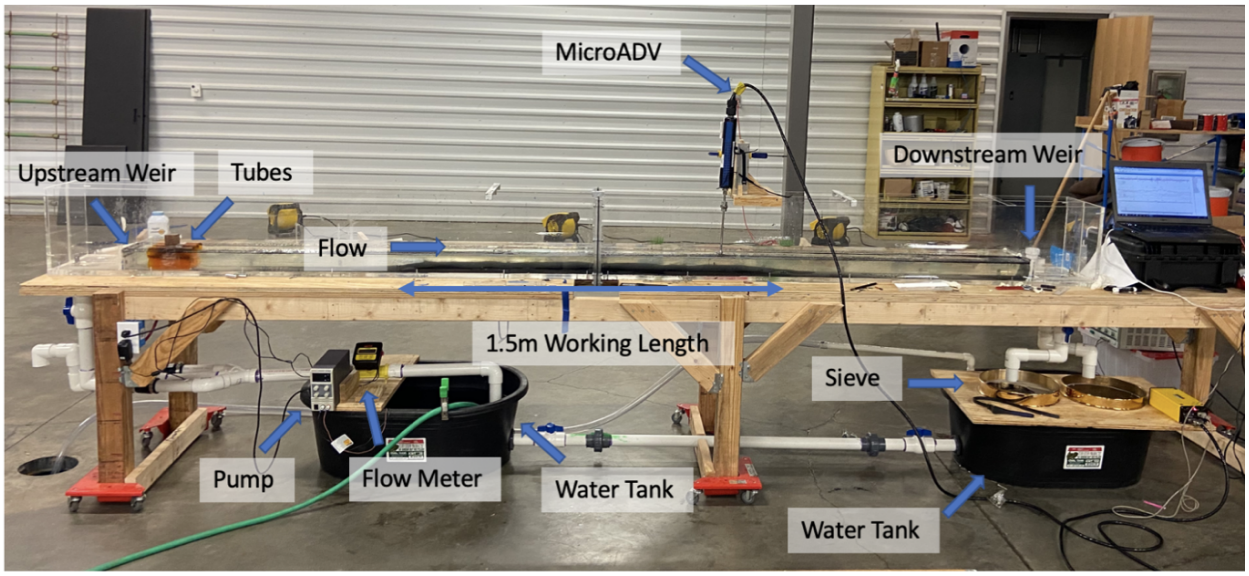

Figure 9. Flume test setup

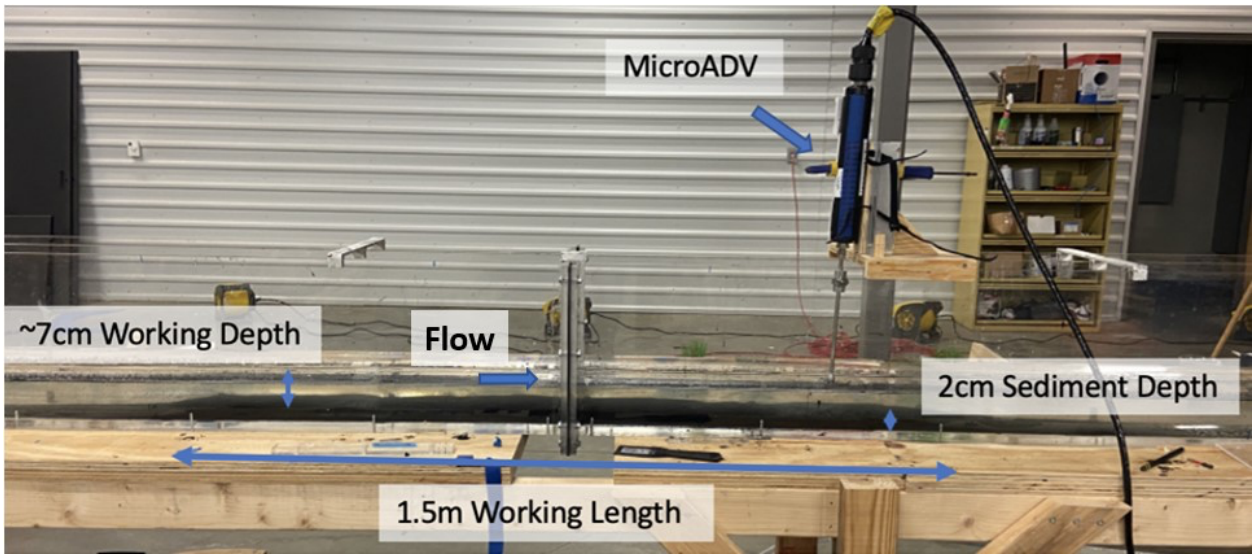

Figure 10. Closer view of flume test setup with sediment and water depths

Upon completion of flume tests, ADV data are exported to readable files and the means and variances of the velocities in the *x*, *y*, and *z* directions are calculated. The turbulent kinetic energy (*TKE*) is calculated using (Pope et al., 2006):

$$TKE = 0.5\rho(\overline{x'^2} + \overline{y'^2} + \overline{z'^2}), \qquad \text{Eq. 2.15}$$

where *x'*, *y'*, and *z'* are the velocity fluctuations in the *x*, *y*, and *z* direction, respectively, and ρ is water density. Bed shear stresses, τ_0, for all conditions, are calculated via (Soulsby, 1983; Stapleton & Huntley, 1995):

$$\tau_0 = 0.19TKE \qquad \text{Eq. 2.16}$$

The dimensionless Shield's parameter, τ_*, is then calculated using:

$$\tau_* = \frac{\tau_0}{\gamma(G-1)D50}, \qquad \text{Eq. 2.17}$$

where γ is the specific weight of water, *G* is the specific gravity of the sediment, and *D50* is the average particle diameter of the sediment, or the diameter of the sediment at which 50% of the particle diameters are larger and 50% are smaller. For the D50 grain size to be representative of the sediment as a whole, the sediment mixture has to be relatively well-sorted, and the area above the sediment grain size gradation curve from D0 to D50 must be greater than one third of the entire area above the curve, i.e., from D0 to D100 (Shields, 1936). This condition is met by all four sediment mixtures. The definition used for the Reynold's particle number, R_p, and subsequent critical Shield's parameter, τ_c^*, are as follows (Parker et al., 2003):

$$R_p = \frac{\sqrt{(G-1)gD50}}{\upsilon} D50 \qquad \text{Eq. 2.18}$$

$$\tau_c^* = \frac{1}{2}\left(0.22R_p^{-0.6} + 0.06 * 10^{-7.7R_p^{-0.6}}\right), \qquad \text{Eq. 2.19}$$

Results from the experiments using the *TKE* method are then compared to calculations based on the 'law of the wall' method and the Reynold's shear stress method. For the law of the wall method, described by von Karman (1930), average velocities are recorded at heights of 1 cm, 1.5 cm, 2 cm, and 2.5 cm above the bed surface at a single flow to produce a velocity profile. These velocities are then plotted against the natural log of their distances from the bed, and a line is fit to the data. The slope, *m*, from that linear equation is then used to estimate the shear velocity, u^*, from the following equation (Dingman, 2009):

$$u^* = \frac{K}{m}, \qquad \text{Eq. 2.20}$$

where *K* is the von-Karman constant of 0.4. From there, bed shear stress, τ_0, is estimated:

$$\tau_0 = \rho u^{*2} \qquad \text{Eq. 2.21}$$

For the Reynold's shear stress method, bed shear stress is estimated by the following equation (Dingman, 2009):

$$\tau_0 = -\rho\overline{u'w'}, \qquad \text{Eq. 2.22}$$

where *u'* and *w'* are the velocity fluctuations in the streamwise and vertical directions, respectively.

2.6. Tracer Sediment Bar Seeding in LMRPM

After the first "50 Years with Combined Operation of the Mid-Breton and Mid-Barataria Sediment Diversions" experiment was completed on the LMRPM, several sediment samples were taken from various locations around the model, including the sand bars 1 mile upstream of both the Mid-Breton and Mid-Barataria sediment diversions (river mile 69.5-68.7, or river kilometer 111.9-110.6 for Mid-Breton and river mile 62.1-61.6, or river kilometer 99.9-99.1 for Mid-Barataria). As a simple qualitative test, about 50 mL of the tracer sediment in the D50 size range

(0.500-0.355 mm) was placed in the sediment bars where each sediment sample had been taken from upstream of the diversions. Then, the hydrograph for Year 46 (historical hydrograph for 2009 in the prototype river) was run through the model at a sea level of 3.3ft NAVD88. This hydrograph was chosen because it has a good variety of flows and conditions on the model (sea-level, bed elevations) were closest to what they were when that year was actually run during the 50-year experiment. During the hydrograph, the lights over the model were turned off and UV flashlights were used to illuminate the tracer sediment. Videos were taken to follow the tracer sediment during particular flows as it became suspended from the sand bars and was transported downstream into and past the sediment diversions. Because only qualitative data were taken (video recordings), the objective of this test was simply to observe how the tracer sediment behaves when implemented in the model and how that compares to the behavior of the model sediment.

Chapter 3. Results

3.1. Chemicals and Agitation Exposure Tests

Sediment sieve analyses showed minor differences in grain size distributions over the 15-day sampling period, suggesting a slight fining of tracer grains occurred (Table 2). It is important to note that standard deviations in the range of 0.001-0.033 mm between samples are not unfounded from small sieve analyses of even the same sample of sediment. This is due to the small quantities of sediment analyzed (<20g) and the relative error associated with the sieves (e.g., sediment released from sieves during shaking, particles stuck in sieve mesh even after cleaning) and sieve scale (+/- 0.01g error). The largest variations were observed in the D90 particle sizes for all samples, which is likely because the coarser particles comprise a smaller percentage of the overall samples, so a small difference in mass percentage will lead to a larger variation in interpolated particle size. Observations, however, demonstrated that the sample exposed to chemicals and agitation (i.e., the sample exposed to conditions most like those of the LMRPM), had much murkier water, most likely due to a minor leaching of the tracer particle coating over time, and should be considered if the tracer is implemented in the LMRPM.

Table 2. Standard deviation in millimeters of sediment samples from Day 0, 5, 10, and 15 from Original dry tracer sediment ("Original"), tracer sediment saturated with water and Tide detergent ("Tide"), tracer sediment saturated with water, Tide detergent, and chlorine bleach ("Tide & Cl"), and tracer sediment saturated with water, Tide detergent, and chlorine bleach and agitated for 2 hours daily ("Tide, Cl, Agitation").

	Original (mm)	Tide (mm)	Tide & Cl (mm)	Tide, Cl, Agitation (mm)
D10	0.002	0.001	0.003	0.003
D50	0.004	0.010	0.010	0.011
D90	0.025	0.032	0.033	0.033

3.2. Porosity and Density Tests

While the tracer sediment was designed to have a specific gravity of 1.05, when mixed with water and laundry detergent (to reduce surface tension), approximately 34% of the tracer sediment, by volume, floated. To extract the higher quality sinking sediment, the tracer sediment was first saturated with water and detergent, mixed several times, and allowed to settle before the floating particles were manually separated from the sinking particles via a finely meshed net. The tracer particles tested in this experiment are therefore the "sinking" particles. It is important to note that the particle density and porosity results are highly sensitive to slight changes in weight or volume, so any losses of water when transferring from beaker to beaker can cause somewhat significant changes in results. With the scale and graduated cylinders, there is an estimated error of +/- 0.1 g and +/- 1 mL, respectively, leading to an error of +/- 0.003 and 0.005 g/cm^3 for the bulk and particle densities, respectively.

Table 3. Porosity, bulk density, and particle density of model and tracer sediments and the percent differences between them.

	Model Sediment	Tracer Sediment	Difference %
Porosity (%)	43.00	35.50	17.44
Bulk Density (g/cm^3)	0.60	0.72	-20.58
Particle Density (g/cm^3)	1.05	1.11	-6.55

The calculated particle density of the tracer sediment is slightly higher than the specified density of 1.05 g/cm^3 (Table 3). It is possible that when measuring this density, the manufacturer calculated the average of all of the particles (both the sinking and floating particles), which amounted to 1.05 g/cm^3. After separating out the floating particles from the sinking particles and drying the samples, a discernible variation in color between the samples is noted (Figure 11).This variation in color suggests that the tracer particles were not uniformly covered in their fluorescent and magnetic coating, and that perhaps, it is this fluorescent and magnetic coating that affects the

density of the particles. This would mean that the sinking particles are denser due to their more thorough coating, and that the floating particles are less dense due to their non-thorough coating.

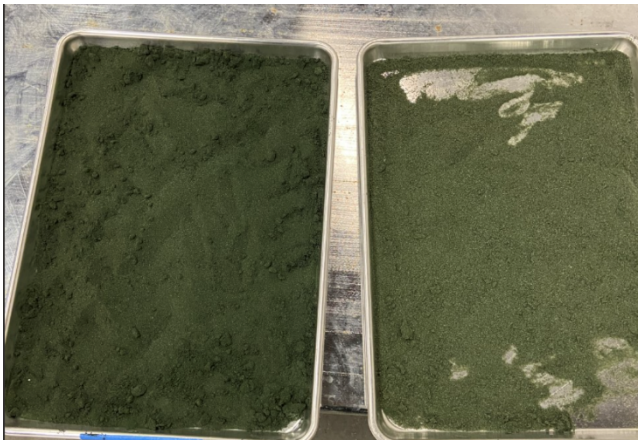

Figure 11. The darker, dried "sinking" tracer sediment on the left and lighter-colored, dried "floating" sediment on the right.

3.3. Settling Velocity Tests

On average, the settling velocities of the tracer sediment are 48% higher than those of the model sediment (Table 4). When compared to their theoretical values (Table 4), all of the recorded settling velocities for each grain size range remain within the limits of calculated theoretical settling velocities per Stokes' formula (Eq. 2.13), and all but the grains in the 0.355-0.15 mm range of the tracer sediment record settling velocities within the calculated limits per Julien's formula (Eq. 2.12). The reason that the calculated theoretical settling velocities vary slightly between the same grain sizes but for different grain size groupings (i.e., the theoretical settling velocity for 0.5 mm for the model sediment is 6.60 mm/s in the 0.85-0.5 mm grouping and then 6.68 mm/s for 0.5 mm in the 0.5-0.355 mm grouping) is because the water temperature was taken before each trial, and slight variations in water temperature affect the water's kinematic viscosity, which is an important variable in both formulas. However, it is important to note that Stokes' formula assumes the settling particles are spherical, which is not the case with the model sediment. Furthermore,

both Stokes' and Julien's equations are valid under the assumption that flow is laminar, or the Reynold's number for each sediment size is less than 1. Calculations of the Reynold's number ranged from 15.78 for 0.85 mm particles to 0.98 for 0.15 mm particles for the tracer sediment and from 7.79 for 0.85 mm particles to 0.42 for 0.15 mm particles for the model sediment. While only the smallest grain sizes achieved Reynolds numbers for laminar flow, the Reynolds numbers were all relatively low, and observed velocities stayed well within range of theoretical values.

Table 4. Calculated theoretical settling velocities from Julien's equation (Eq. 2.12) and Stokes' equation (2.13) for grain sizes 0.85mm, 0.5mm, 0.355mm, and 0.15mm compared to observed settling velocities for general grain size ranges of 0.85-0.5mm, 0.5-0.355mm, and 0.355-0.15mm from tests for both the model and tracer sediments.

	Model Sediment			Tracer Sediment		
Grain Size (mm)	Julien Theor. Velocity (mm/s)	Stokes Theor. Velocity (mm/s)	Obs. Velocity (mm/s)	Julien Theor. Velocity (mm/s)	Stokes Theor. Velocity (mm/s)	Obs. Velocity (mm/s)
0.85	11.84	19.08	9.46	20.27	40.88	19.69
0.5	5.63	6.60		10.73	14.14	
0.5	5.68	6.68	5.45	10.76	14.20	8.32
0.355	3.15	3.36		6.32	7.16	
0.355	3.18	3.40	2.82	6.44	7.34	6.73
0.15	0.60	0.61		1.29	1.31	

The fact that both the model and tracer sediment particles recorded settling velocities within range of their calculated theoretical values corroborates the particle densities calculated from the porosity and density experiments, considering the density of the particles was the only significant variable that changed when comparing the model and tracer sediments theoretical settling velocities. As seen in Table 4, the 6% increase in particle density from the 1.05 g/cm^3 of the model sediment to the 1.11 g/cm^3 of the tracer sediment resulted in the tracer sediment having calculated theoretical settling velocities more than double that of the model sediment.

3.4. Angle of Repose Tests

The Model Full Range sediment had the highest angle of repose of the sediment mixtures at 57.2° and the Tracer D50 exhibited the lowest angle of repose at 32.2° (Table 5). The angle of

repose of the Tracer D50 sediment is about 42% lower than that of the Model D50 sediment. The lower angle of repose for the tracer sediment is due to the fluid-like behavior of the sediment that is likely caused by the sphericity and slightly higher density of the tracer sediment particles when compared to the model sediment. The angular, shard-like pieces of model sediment (Figure 6) are more likely to interlock with one another, preventing sliding and rolling when the jar is rotated. This leads to the model sediment's higher angles of repose observed during testing.

The Model Full Range mixture exhibited a 1.9° higher angle of repose and 1.6° higher standard deviation than the Model D50 sediment, which is likely due to the wider range of grain sizes that both aides in the interlocking capabilities of grains and increases the variability of results. Interestingly, the Tracer & Model Mix had an angle of repose between those of the model and tracer sediments. At 48°, the Tracer & Model Mix angle of repose is only 16% lower than that of the Model Full Range. This suggests that when the tracer and model sediments are mixed together, the difference in angle of repose between the particles decreases, and the mixture exhibits behavior similar to that of the Model Full Range sediment.

Table 5. Average measured angle of repose of four different sediment mixtures and their standard deviations from 6 trials.

	Model Full Range	Model D50	Tracer D50	Tracer & Model Mix
Angle of Repose	57.2°	55.3°	32.2°	48.0°
St. Dev	5.6°	4.0°	2.6°	4.6°

3.5. Incipient Motion Tests

All ADV files were imported to MATLAB version 2018b, where they were first despiked using a toolbox from Mori et al. (2007) who modified the original method from Goring and Nikora (2002) that uses a phase-space method to flag and remove unnatural spikes in each recording due

to error associated with the ADV. A script was written to calculate the average, standard deviation, and variance of the x, y, and z velocities, along with the *TKE*, τ_0, τ_*, and average correlation percentage and signal to noise ratio. A script structure created by Julian Traphagan (2023) at Louisiana State University was used to automatically run all of these calculations and plot the x, y, and z velocities along with their stationarities for each ADV recording. This process made it possible to remove any recordings that were unusable (i.e., that had velocities that did not make sense (close to zero) for their corresponding flow or did not achieve stationarity). Figure 12 is an example of the MATLAB output for a single recording at a given voltage.

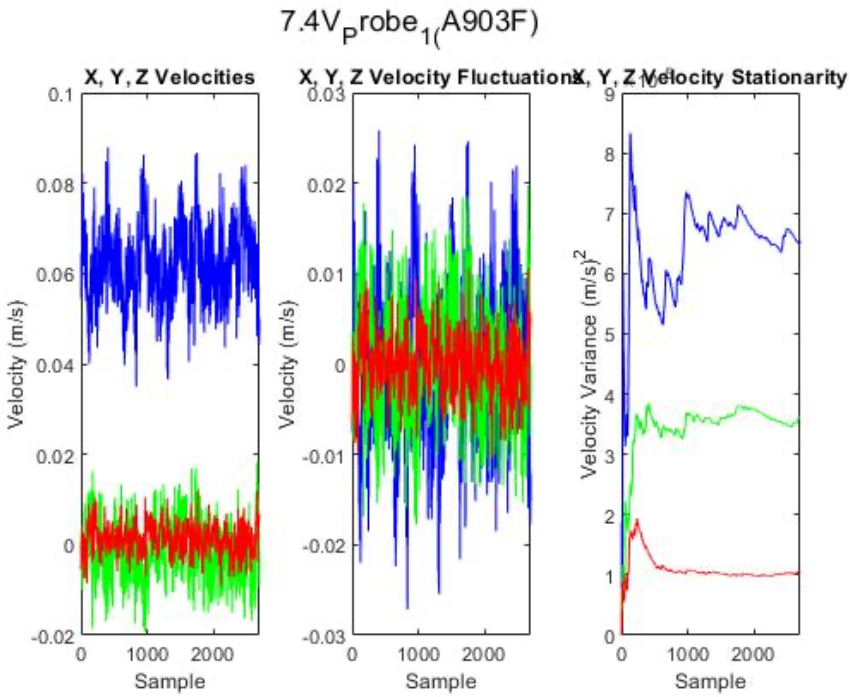

Figure 12. Example MATLAB output for 90 second ADV recording, sampling 30 times a second, conducted at 7.4 volts during Trial 1 of the Model D50 sediment. Blue represents ADV measurements in the x, or streamwise direction, green in the y, or lateral direction, and red in the z or vertical direction. The graph on the left depicts the ADV velocity in the x, y, and z directions for all 2700 samples, the middle graph depicts the velocity fluctuations from the mean in the x, y, z directions for all 2700 samples, and the graph on the right depicts the stationarity of the velocity measurements, or the velocity variance over the course of the 2700 samples.

From there, ADV data were combined with observational data in tables and color-coded to represent when motion was observed from the particles. As mentioned earlier, incipient motion of

particles was considered as the point at which several particles were observed rolling, sliding, or saltating throughout the majority of the ADV recording.

All ADV data files were found to have average correlation percentages in the range of 96.7-99.1%, and average Signal to Noise ratios (SnR) in the range of 21.2-36.3 decibels, which is considered above the satisfactory suggestions of 70% and 20 decibels, respectively (Sontek, 2001).

3.5.1. Model Sediment Full Size Range

The first group of experiments utilized the full grain size distribution of the LMRPM model sediment, referred to as "Model Full Range". To make this distribution, batches of coarse and fine sediment are analyzed via sieves to measure their sediment size gradations. Then, depending on these gradations, certain amounts of the coarse and fine sediments are mixed together. Finally, the new mixture undergoes a new sieve analysis to determine the final grain size distribution and the D10, D50, and D90 grain sizes are compared to the target values for the model sediment mixtures that are typically injected into the model (Table 6).

Table 6. Grain size distribution (observed diameter) for sediment used in the Model Sediment Full Size Range incipient motion experiments, as compared to the "Target Diameter" of model sediment generally used in LMRPM experiments.

Grain Size Fraction	Target Diameter (mm)	Observed Diameter (mm)
D10	0.25	0.24
D50	0.40-0.45	0.45
D90	0.80	0.80

Trial 1 of the Model Full Range experiment was used to test the ADV and ensure that it was reading good measurements with the probe at a distance of 8 cm from the flume bottom to record velocities in the 0-1 cm range from the bed. Results from this first trial produced velocities that were nonsensical when compared to the theoretical cross-sectional average velocities based on the discharge from the flow meter (hovering around 0 m/s), so the probe height was increased

to 8.5 cm (reading velocities in the 0.5-1.5cm range above the bed), and ADV readings improved. All remaining trials for all 4 experiments were conducted with the ADV probe at this height.

Shields parameters from Trials 2 through 5 are plotted along with the critical Shield's dimensionless shear stress thresholds notated as "τ_c*" (Figure 13). Because water from the tap was used, it was difficult to control the water temperature from trial to trial. For trials T2-T5, water temperatures varied from a maximum of 24 degrees Celsius during Trial 5 to a minimum of 19.5 degrees during Trial 3. The difference in temperature causes a somewhat considerable difference in calculated critical Shield's values, so both values are plotted in Figure 13 to represent a critical threshold for T2-T5. However, the difference in temperature did not cause a significant difference in *TKE* and resultant bed shear stress and dimensionless Shields values, so all bed shear stresses and dimensionless Shields values were calculated with the water density at 20 degrees Celsius, which is 998 kg/m^3.

From visual observations and Figure 13, it can be estimated that incipient motion of particles begins around a streamwise velocity of 0.064 m/s and a dimensionless Shields parameter of about 0.034. While these are the average values, it is evident that Trial 4 introduces more variation when compared to the other trials. For example, at the same velocity of approximately 0.073 m/s, trial 4 has a τ* of 0.023, while Trial 2 has a τ* of 0.061, representing a 66% difference in τ*. This variation is also seen in the bed shear stresses, τ_0, with increasing streamwise velocities (Figure 14). The lower τ* and τ_0 values are due to the lower variances of the velocities in the x direction when compared to Trials 2-3 and 5 (Figure 15).

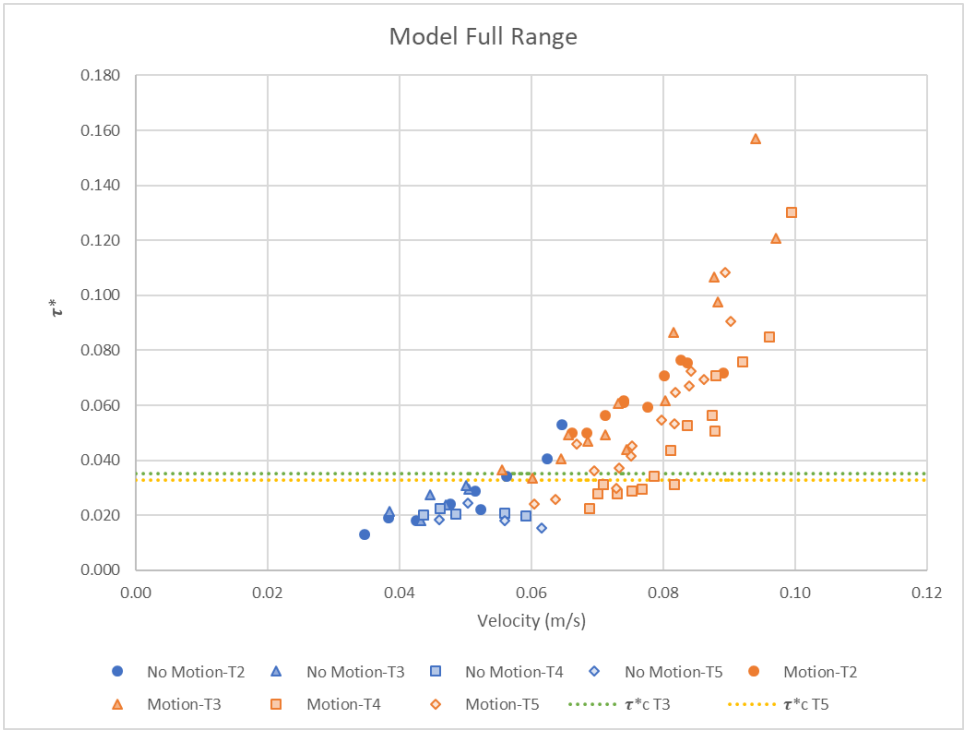

Figure 13. Average ADV x velocity of each ADV recording from 4 trials of Model Full Range incipient motion tests (T2-T5) and their respective calculated dimensionless Shields parameters, τ*. The blue shades represent no motion of particles observed during the majority of the recording, and the orange shades represent motion observed during the majority of the recording. The dotted lines represent the upper and lower limits of calculated critical Shields thresholds for incipient motion, τ_c*, that vary due to differing temperatures, and subsequent densities and kinematic viscosities of the water during different trials.

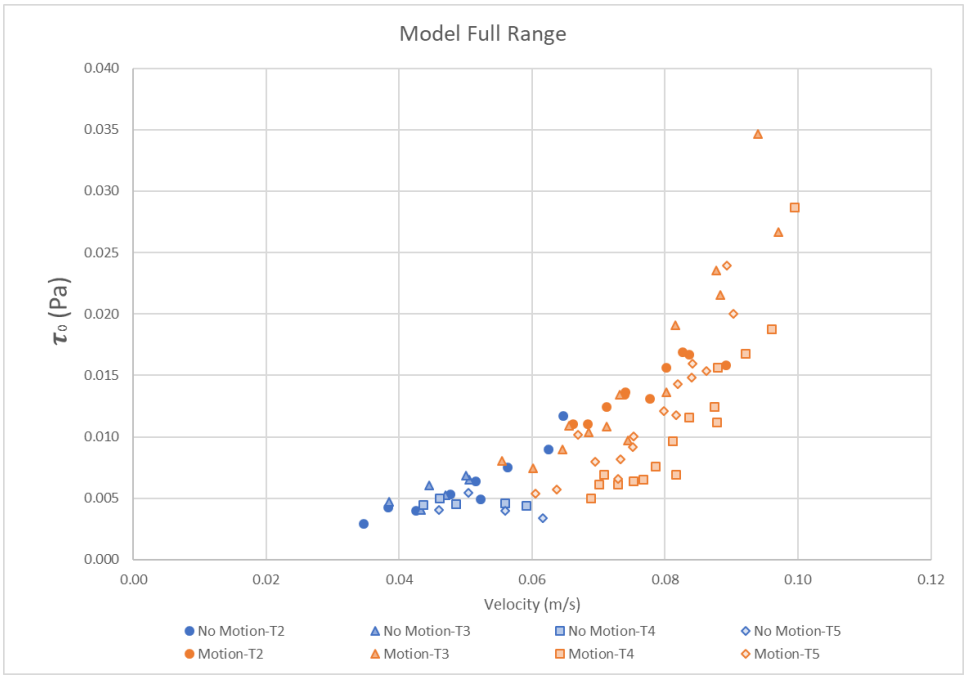

Figure 14. Average ADV x velocity of each ADV recording from 4 trials of Model Full Range incipient motion tests (T2-T5) and their respective calculated bed shear stresses, τ_0, in Pascals. The blue shades represent no motion of

particles observed during the majority of the recording, and the orange shades represent motion observed during the majority of the recording.

The lower variances for T4 and T5 (Figure 15) could be due to a slight difference in the sediment beds when compared to those of T2 and T3 (Figure 16). There appears to be minor bedforms in T2 and T3 in the vicinity of the ADV probe, while the beds near the probe in T4 and T5 appear to be much flatter. The presence of bedforms leads to flow separation and the formation of eddies due to increased form drag at the bed surface, which subsequently increases local downstream turbulence (Kleinhans et al., 2017). This error was introduced because the beds were screeded flat manually, and while small variations in bed are more obvious in a magnified video, they were missed by the naked eye. Furthermore, the pronounced scatter seen in this experiment (Figure 13-Figure 15) can be generally associated with the unpredictability of turbulent flow that causes short-term pressure gradients and other fluctuating hydrodynamic forces that can all lead to varying bed shear stresses regardless of their corresponding velocities (Agudo et al., 2017).

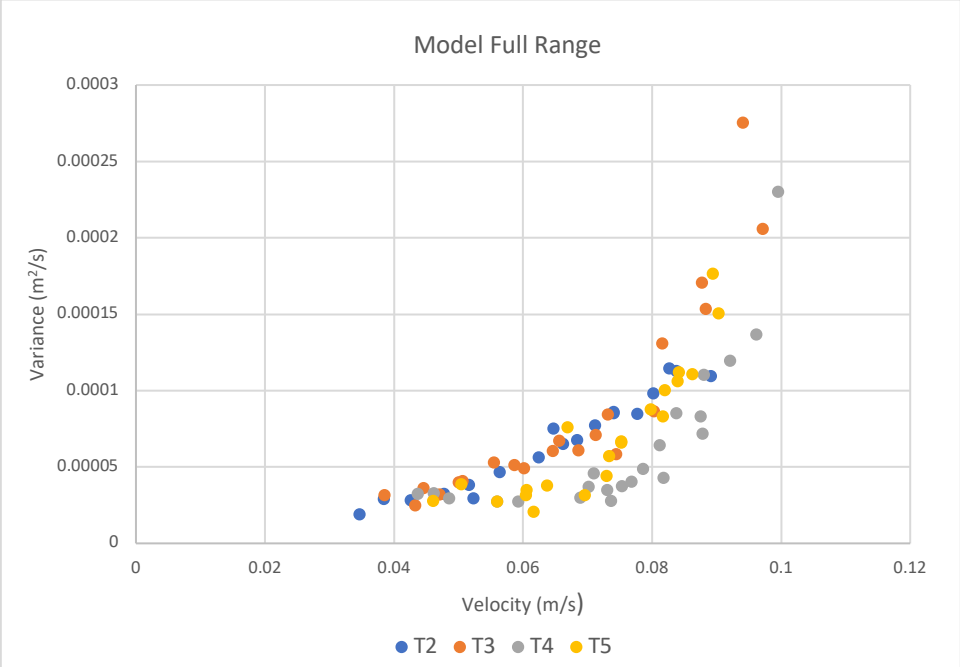

Figure 15. Variance of ADV velocity measurements in the x (streamwise) direction with corresponding average ADV velocities in the x direction for all observed flows in Trials 2-5 (T2-T5) in the Model Full Range incipient motion experiment.

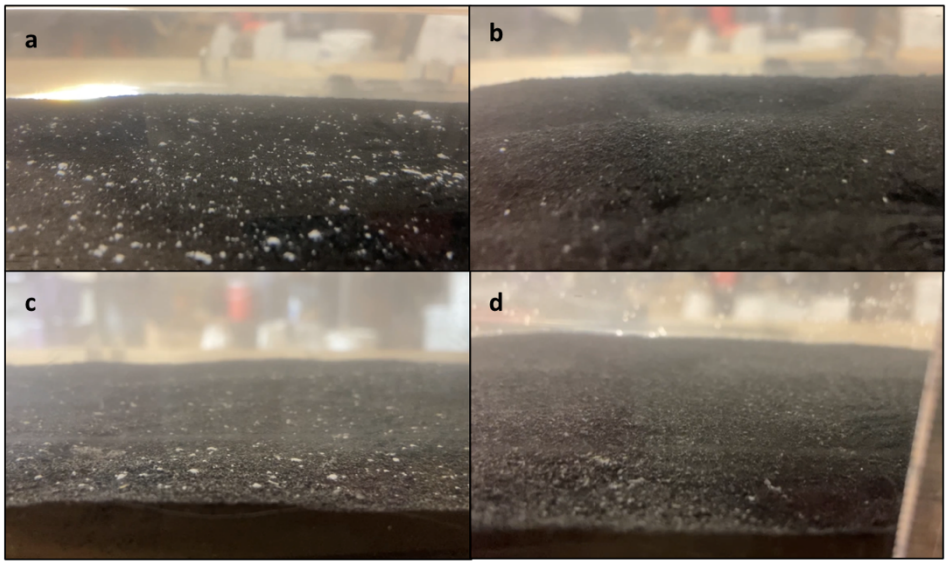

Figure 16. Close-up view of bed surface by ADV probe as seen in observational video recordings from Model Full Range incipient motion experiments a) Trial 2, b) Trial 3, c) Trial 4, and d) Trial 5.

3.5.2. Model Sediment D50 Size Range

The second experiment was run using LMRPM sediment in the D50 range (0.355-0.50 mm). This size fraction was created by sieving the Model sediment through a No. 35 (0.50 mm) and No. 45 (0.35 mm) sieve and then conducting a small sieve analysis on the new mixture. The results of this sieve analysis are in Table 7. Of particular importance is that the D50 is the same size as the D50 for the Model Full Range experiment. The small sieve analysis utilizes a No. 30 and No. 45 sieve instead of a No. 35 sieve, so the sieve analysis result of 0.56 mm for the D90 is not necessarily accurate due to interpolation.

Table 7. Grain size distribution (observed diameter) for sediment used in the Model D50 sediment incipient motion experiments, as compared to the "Target Diameter" of model sediment generally used in LMRPM experiments.

Grain Size Fraction	Target Diameter (mm)	Observed Diameter (mm)
D10	0.25	0.33
D50	0.40-0.45	0.44
D90	0.80	0.56

For trials T1-T3, water temperatures varied from a maximum of 25.9 degrees Celsius during Trial 1 to a minimum of 20.1 degrees during Trial 2. The difference in temperature causes a somewhat significant difference in calculated critical Shield's values, so both values are plotted in Figure 17 to represent a critical threshold for T1-T3. Incipient motion of particles is estimated to occur at a streamwise velocity of around 0.056 m/s, a Shields parameter of 0.04 (Figure 17), and a bed shear stress of 0.009 Pa (Figure 18). On average, the Shields stresses and bed shear stresses between all three trials remained relatively close to one another. The most significant differences were between Trial 2 and 3 and occurred at the higher velocities throughout the experiment, specifically in the 0.06-0.08 m/s velocity range. At an ADV velocity of about 0.072 m/s, Trial 2 recorded a bed shear stress and Shields parameter almost twice that of Trial 3 at the same velocity. While this is most likely due to a higher variability in turbulence that occurs with higher flows, slight differences in bed topography could also cause this discrepancy, as bed shear stress and Shields parameters remain consistently lower for Trial 3 when compared to Trial 2.

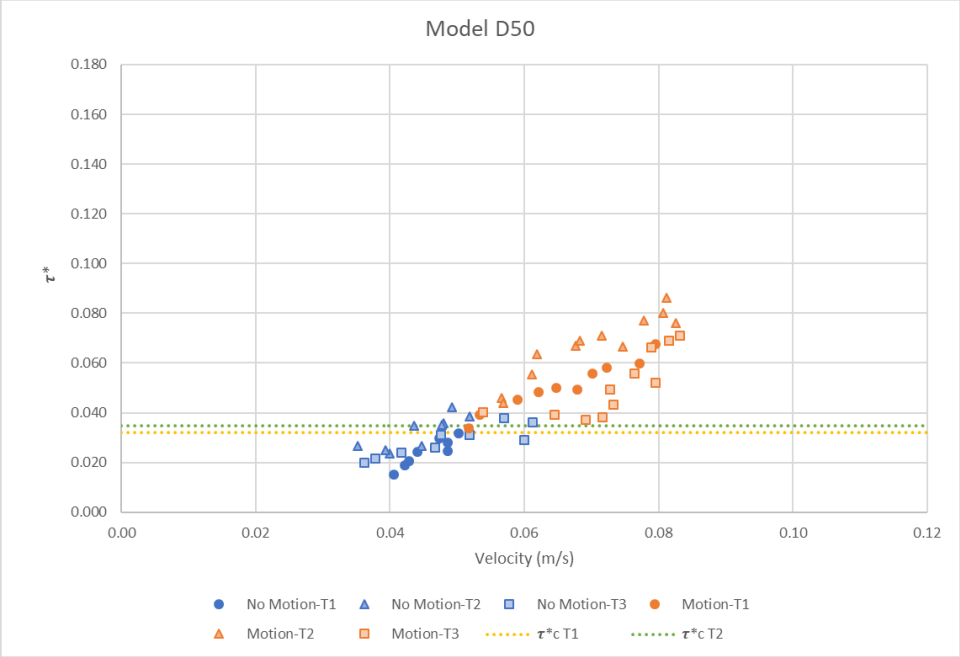

Figure 17. Average ADV x velocity of each ADV recording from 3 trials of Model D50 incipient motion tests (T1-T3) and their respective calculated dimensionless Shields parameters, τ*. The blue shades represent no motion of

particles observed during the majority of the recording, and the orange shades represent motion observed during the majority of the recording. The dotted lines represent the upper and lower limits of calculated critical Shields thresholds for incipient motion, τ_c*.

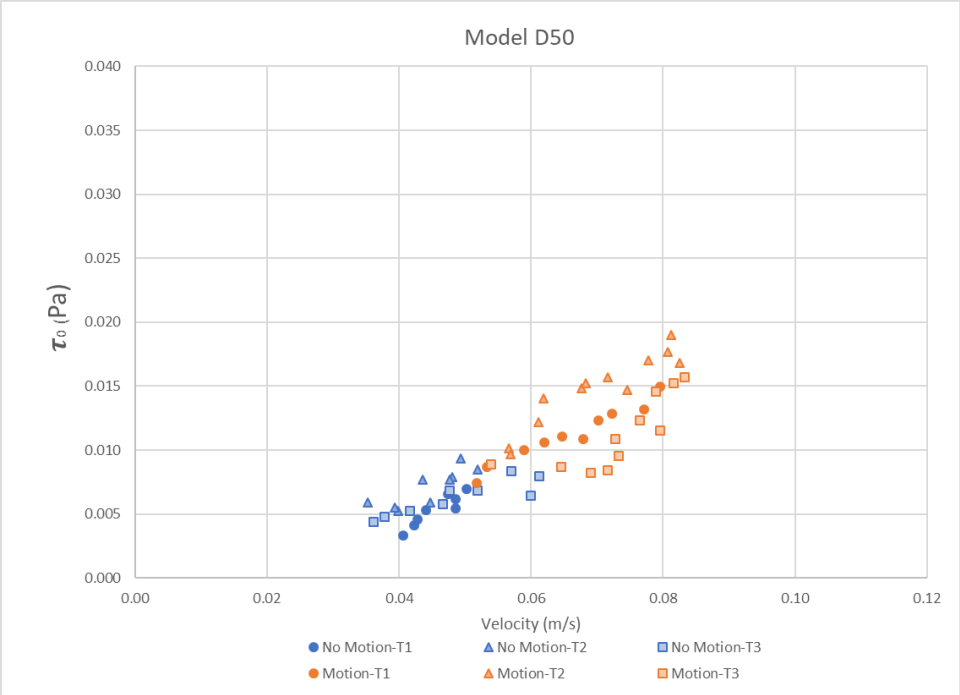

Figure 18. Average ADV x velocity of each ADV recording from 3 trials of Model D50 incipient motion tests (T1-T3) and their respective calculated bed shear stresses, τ_0, in Pascals. The blue shades represent no motion of particles observed during the majority of the recording, and the orange shades represent motion observed during the majority of the recording.

3.5.3. Tracer Sediment D50 Size Range

The third experiment was run using tracer sediment in the D50 range of the LMRPM model sediment (0.355-0.50 mm). This sediment was mixed by sieving the tracer sediment through a No. 35 (0.50 mm) and No. 45 (0.35 mm) sieve and then conducting a small sieve analysis on the new mixture (Table 8). Of particular importance is that the D50 is the same size as the D50 for the Model Full Range and the Model D50 experiment. Like with the Model D50 sediment, the sieve analysis result of 0.56 mm for the D90 is not necessarily accurate due to interpolation between the No. 30 and No. 45 sieve amounts.

Table 8. Grain size distribution (observed diameter) for sediment used in the Tracer D50 sediment incipient motion experiments, as compared to the "Target Diameter" of model sediment generally used in LMRPM experiments.

Grain Size Fraction	Target Diameter (mm)	Observed Diameter (mm)
D10	0.25	0.32
D50	0.40-0.45	0.44
D90	0.80	0.56

For Trial 1, it was very difficult to discern when incipient motion began. At some of the first discharges, particles were already seen in motion, but were floating downstream close to the bed instead of rolling, sliding, or saltating. With increasing discharges, the number of particles floating at the bed surface only increased and made the discernment of incipient motion increasingly difficult. After almost 2 hours, the number of floating particles seemed to decrease, and the flow was lowered to one of the beginning low flows. At this point, the floating particles were no longer an issue, and the experiment continued, with an improved ability to observe incipient motion. A few more recordings were taken without the floating particles and then the experiment resumed the following day, after ensuring the bed was screeded flat and the sediment was "fluffed" again. These two separate days of the trial are referred to as Tracer D50 Trial 1 Part 1 and Part 2. For the second part of the trial, the floating tracer particles had already been flushed out of the flume, so the point of incipient motion was much easier to discern. These "floater" particles were captured by the sieve at the downstream outlet of the flume and thrown away (instead of being remixed into the sediment) before the subsequent trials. For the following 2 trials of the Tracer D50 experiment, a low flow was run through the flume for about 30 minutes after the sediment was "fluffed" until all floating particles appeared to have washed out. This did not cause any notable changes in the sediment bed.

For trials T1-T3, water temperatures varied from a maximum of 25.9 degrees Celsius during Trial 2 to a minimum of 19.1degrees during Trial 1 Part 2. The difference in temperature

causes a somewhat significant difference in calculated critical Shield's values, so both values are plotted to represent a critical threshold for T1-T3 (Figure 19). Incipient motion of particles was observed to occur around an average velocity of 0.043 m/s and at a bed shear stress of 0.005 Pa (Figure 21). On average, the Shields parameters and bed shear stresses remained relatively close to one another between trials, and the velocities for incipient motion were very similar for all three trials (standard deviation of 0.0002 m/s), representing good reproducibility for the Tracer D50 experiment.

The average value for dimensionless Shields stress was 0.025 when calculated with the specific gravity of the model sediment (1.05) and 0.011 when calculated with the specific gravity calculated in the density experiment (1.11) (Figure 19 and Figure 20). The motion of the tracer particles when considered with a lower specific gravity occurs much closer to the Shields critical threshold for motion, τ_c* T2 and τ_c* T1P2 (Figure 19) when compared to the motion of the particles calculated with a higher specific gravity (Figure 20). These figures are juxtaposed to postulate that while the tracer sediment has a higher density than the model sediment, perhaps not all of the tracer particles share the same density. As seen in Figure 7 and Figure 11, the tracer particles do not show a uniform coating of their fluorescent and magnetic paint. If this paint is what dictates the density of the particles, then it is possible that the tracer sediment density is not uniformly 1.11 g/cm^3. Therefore, it is possible that the first particles in motion are those of the lower specific gravity. While the exact specific gravity of the mobile tracer sediments in this experiment cannot be assumed, when tested with the same specific gravity as the model sediment, observational data align better with calculated critical thresholds. It is possible that if the tracer sediment Shields parameters were to be calculated with a specific gravity slightly lower than the

1.05 of the model sediment, observational data might align even better with calculated critical thresholds.

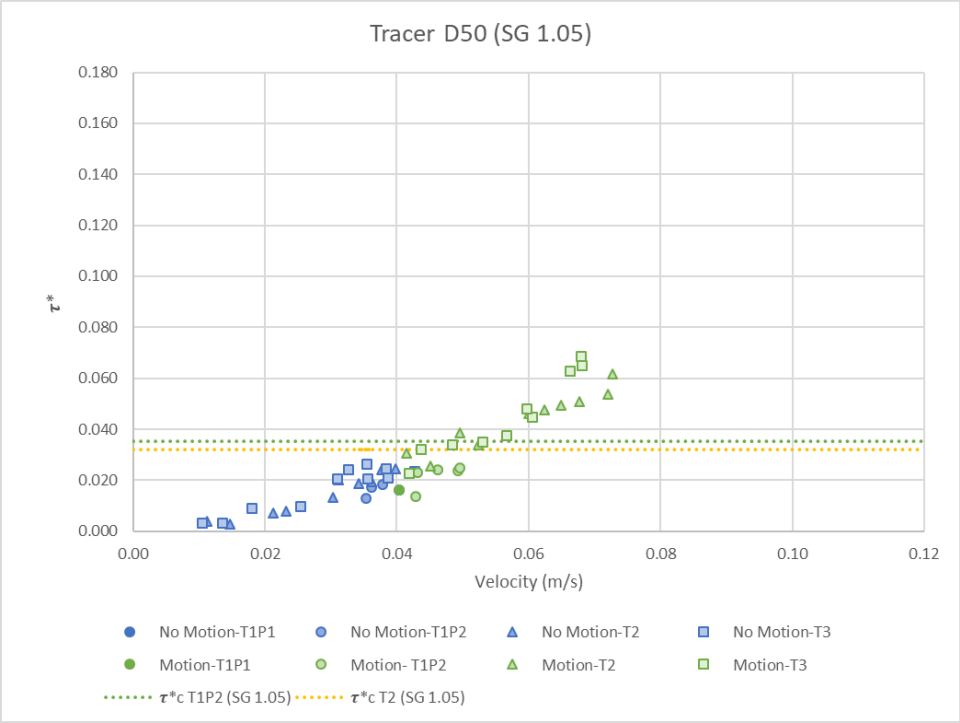

Figure 19. Average ADV x velocity of each ADV recording from 3 trials of Tracer D50 incipient motion tests (T1-T3) and their respective calculated dimensionless Shields parameters, τ*, using a sediment specific gravity (SG) of 1.05. Trial 1 is divided into Trial 1 Part 1 (T1P1) and Trial 1 Part 2 (T1P2). The blue shades represent no motion of particles observed during the majority of the recording, and the green shades represent motion observed during the majority of the recording. The dotted lines represent the upper and lower limits of calculated critical Shields thresholds for incipient motion, τ_c*.

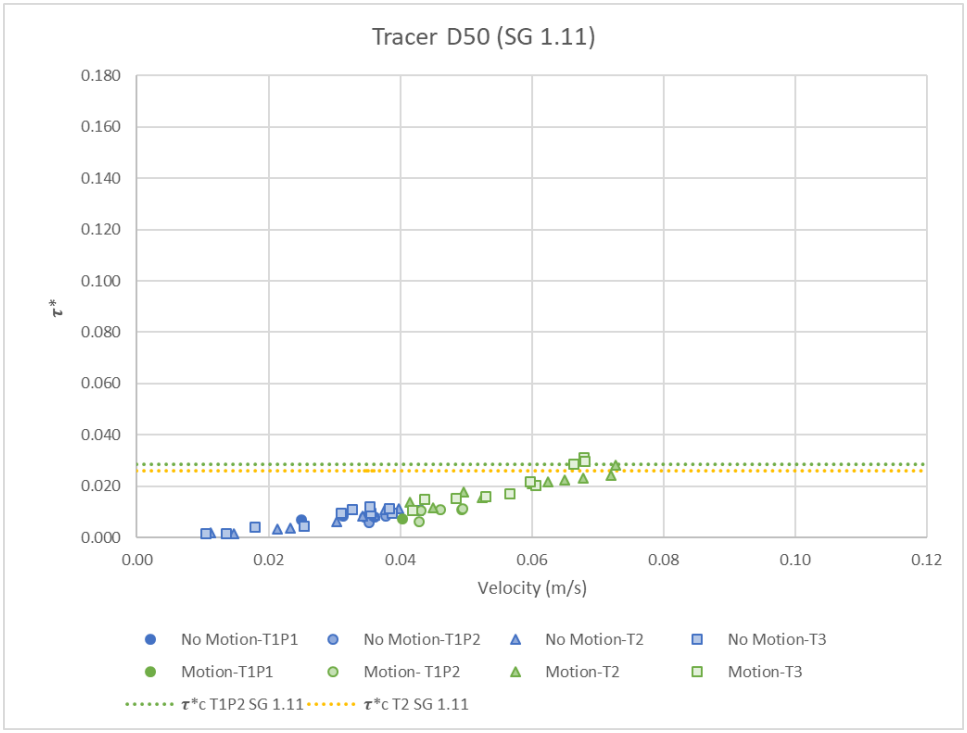

Figure 20. Average ADV x velocity of each ADV recording from 3 trials of Tracer D50 incipient motion tests (T1-T3) and their respective calculated dimensionless Shields parameters, τ*, using a sediment specific gravity (SG) of 1.11. Trial 1 is divided into Trial 1 Part 1 (T1P1) and Trial 1 Part 2 (T1P2). The blue shades represent no motion of particles observed during the majority of the recording, and the green shades represent motion observed during the majority of the recording. The dotted lines represent the upper and lower limits of calculated critical Shields thresholds for incipient motion, τ_c*.

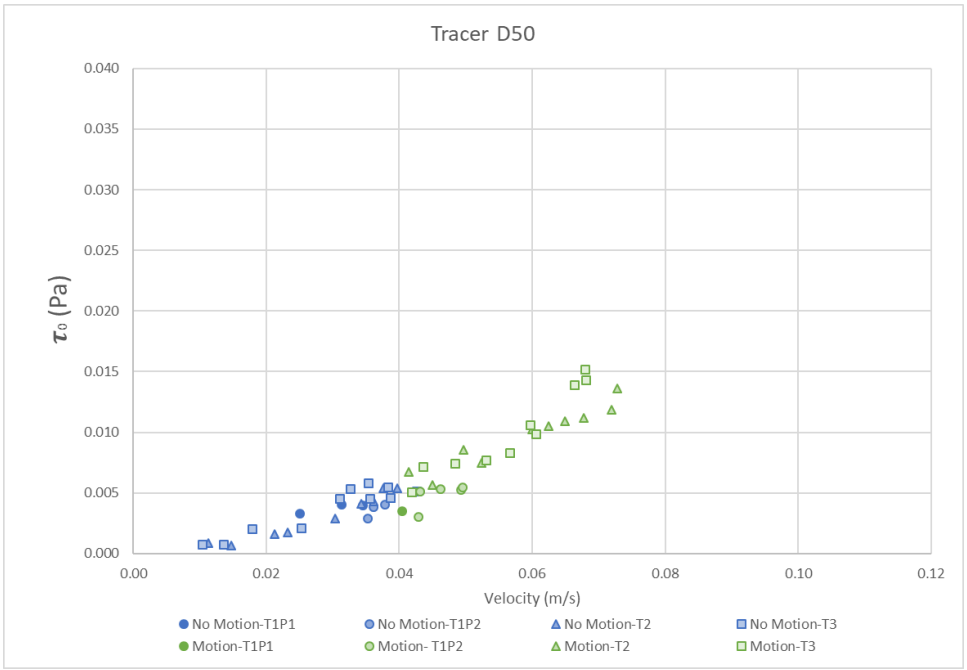

Figure 21. Average ADV x velocity of each ADV recording from 3 trials of Tracer D50 incipient motion tests (T1-T3) and their respective calculated bed shear stresses, τ_0, in Pascals. The blue shades represent no motion of particles

observed during the majority of the recording, and the green shades represent motion observed during the majority of the recording.

3.5.4. Tracer and Model Sediment Mix

For the fourth experiment, the sediment from the Model Full Range experiment was dried and sediment in the D50 range was sieved out using No. 35 and No. 45 sieves. Then, tracer sediment of the D50 size range (0.355-0.500 mm) was added to the mixture, effectively replacing the model D50 sediment fraction of the model full range sediment. The tracer and model sediment mix was then analyzed by sieves, and certain amounts of different sizes of model sediment were added to push the sediment size gradation closer to the target values for the model sediment (Table 9).

Table 9. Grain size distribution (observed diameter) for sediment used in the Tracer & Model Mix incipient motion experiments, as compared to the "Target Diameter" of model sediment generally used in LMRPM experiments.

Grain Size Fraction	Target Diameter (mm)	Observed Diameter (mm)
D10	0.25	0.21
D50	0.40-0.45	0.44
D90	0.80	0.79

For Trial 1 of the Tracer & Model Mix experiment, there was a similar issue with the floating tracer particles disrupting the observations of incipient motion of particles. In the beginning of Trial 1, Tracer particles were floating very close to the bed surface, making it difficult to determine whether they were exhibiting incipient motion or if they were simply lighter "floating" particles that had been suspended upstream. After about 2 hours, all floating particles had been washed out, and incipient motion was easier to discern. For the remaining trials, a low flow was injected into the flume at the start of each trial for about 30 minutes until all floating particles were washed out. This improved the subsequent observational data and did not cause any notable changes in the sediment bed.

For trials T1-T3, water temperatures varied from a maximum of 19.7 degrees Celsius during Trial 1 to a minimum of 19.2 degrees during Trial 2. The minor difference in temperature between these 3 trials did not cause a significant difference in calculated critical Shield's values (0.0351 vs. 0.0354), but both values are plotted to represent a critical threshold for T1-T3 (Figure 22-Figure 23). The tracer began to move at an average velocity of 0.051 m/s, with a bed shear stress of 0.007 Pa. When calculated with the same specific gravity as the model sediment (1.05), the tracer sediment moved at an average dimensionless Shields parameter of 0.030 (Figure 22) compared to an average of 0.014 when calculated with the higher specific gravity of 1.11 from the density experiment (Figure 23). Observational data show that motion of all particles occurs at Shields parameters well below the critical Shields parameter of 0.028 in this scenario. In fact, the calculated critical Shields parameter for this scenario coincided with observed suspension of both tracer and model sediments, suggesting that observational data do not align well with calculated Shields parameters at the higher specific gravity. This fact corroborates the use of the density of 1.05 g/cm^3 for incipient motion calculations regarding the tracer sediment and tracer and model sediment mixes.

When plotted with the specific gravity of 1.05, the model sediment began to move with the tracer sediment at an average velocity of 0.061 m/s with an average dimensionless Shields parameter of 0.042 (Figure 22) and bed shear stress of 0.009 Pa (Figure 24). Therefore, the difference in velocities, Shields parameters, and bed shear stresses to incite motion for model sediment particles as compared to tracer sediment particles when the two are mixed together is about 0.01 m/s, 0.012, and 0.002 Pa, respectively.

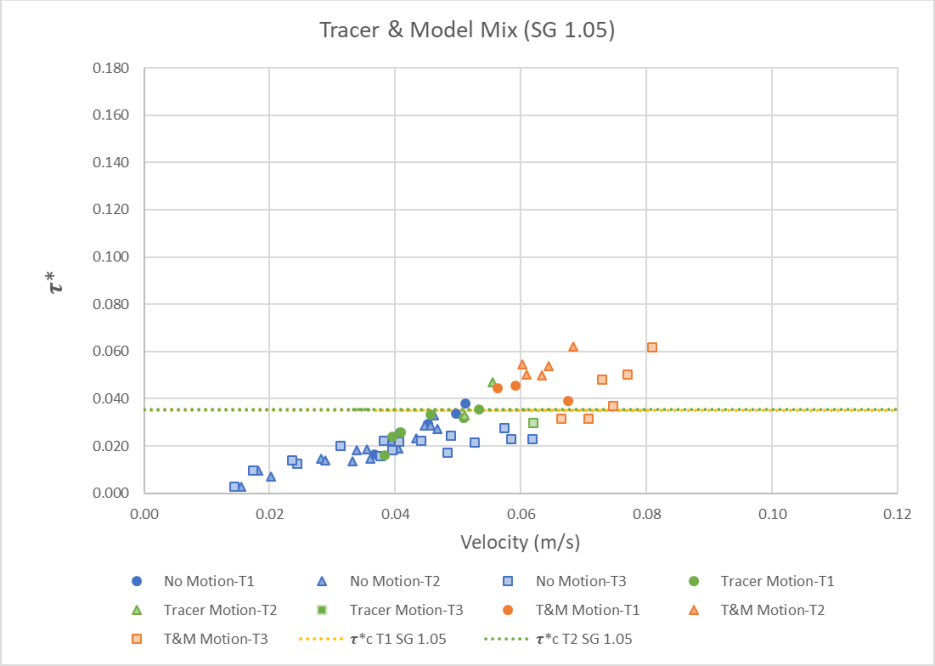

Figure 22. Average ADV x velocity of each ADV recording from 3 trials of Tracer & Model Mix incipient motion tests (T1-T3) and their respective calculated dimensionless Shields parameters, τ*, using a sediment specific gravity of 1.05. The blue shades represent no motion of particles observed during the majority of the recording, the green shades represent motion of tracer particles, and the orange shades represent motion of both tracer and model sediment particles. The dotted lines represent the upper and lower limits of calculated critical Shields thresholds for incipient motion, τ_c*.

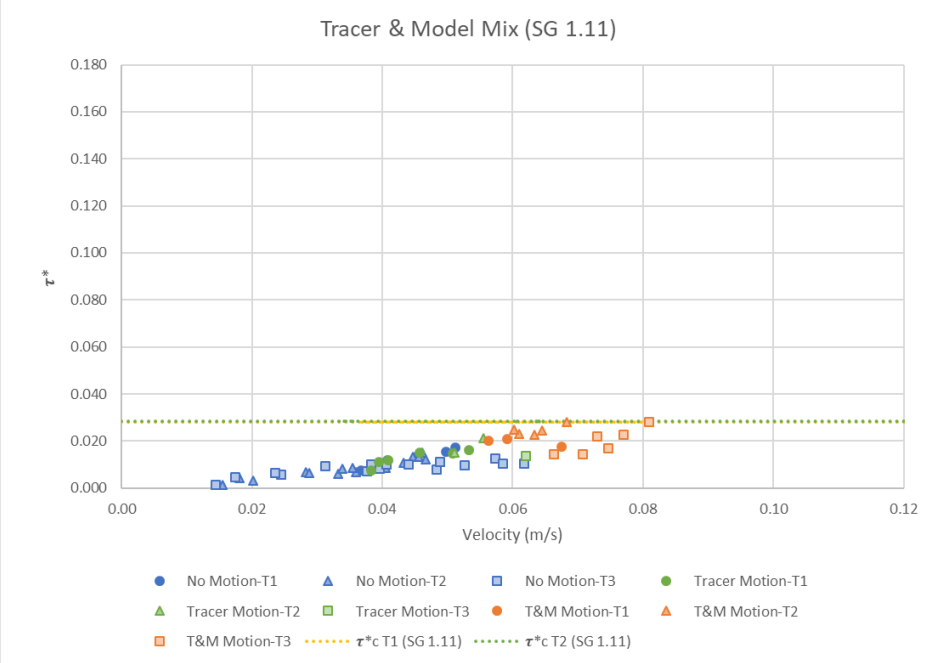

Figure 23. Average ADV x velocity of each ADV recording from 3 trials of Tracer & Model Mix incipient motion tests (T1-T3) and their respective calculated dimensionless Shields parameters, τ*, using a sediment specific gravity

of 1.11. The blue shades represent no motion of particles observed during the majority of the recording, the green shades represent motion of tracer particles, and the orange shades represent motion of tracer and model sediment particles. The dotted lines represent the upper and lower limits of calculated critical Shields thresholds for incipient motion, τ_c*.

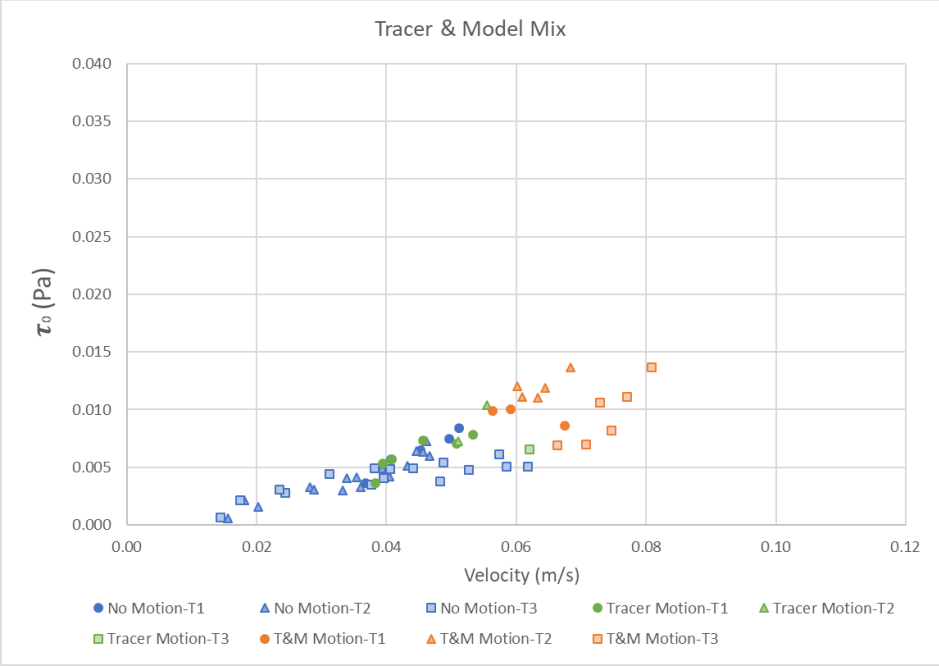

Figure 24. Average ADV x velocity of each ADV recording from 3 trials of Tracer & Model Mix incipient motion tests (T1-T3) and their respective calculated bed shear stresses, τ_0, in Pascals. The blue shades represent no motion of particles observed during the majority of the recording, the green shades represent motion of tracer particles, and the orange shades represent motion of both tracer and model sediment particles.

The sudden drop off in dimensionless shields parameters around 0.068 m/s for Trial 1 and the consistently lower dimensionless Shields parameters for Trial 3 after about 0.05 m/s (Figure 22) can be explained by the lower variances in the streamwise velocities, depicted in Figure 25. At the lower velocities (below 0.05 m/s), all three trials produce variances within range of one another. This suggests that a difference in bed structure between the trials may not be the reason for these trends. Pictures of the bed surface by the ADV probe (Figure 26) show slight differences in topography between Trial 1, 2, and 3. The bed surface of Trial 3, however, appears to have the most varying topography when compared to the other trials, which might usually be associated with inducing more turbulence and thus higher variances, which is not the case. Therefore, it is

possible that the pump simply performed better during Trial 3, in that it maintained a more constant flow, with less fluctuations in discharge that could result in lower variances for Trial 3.

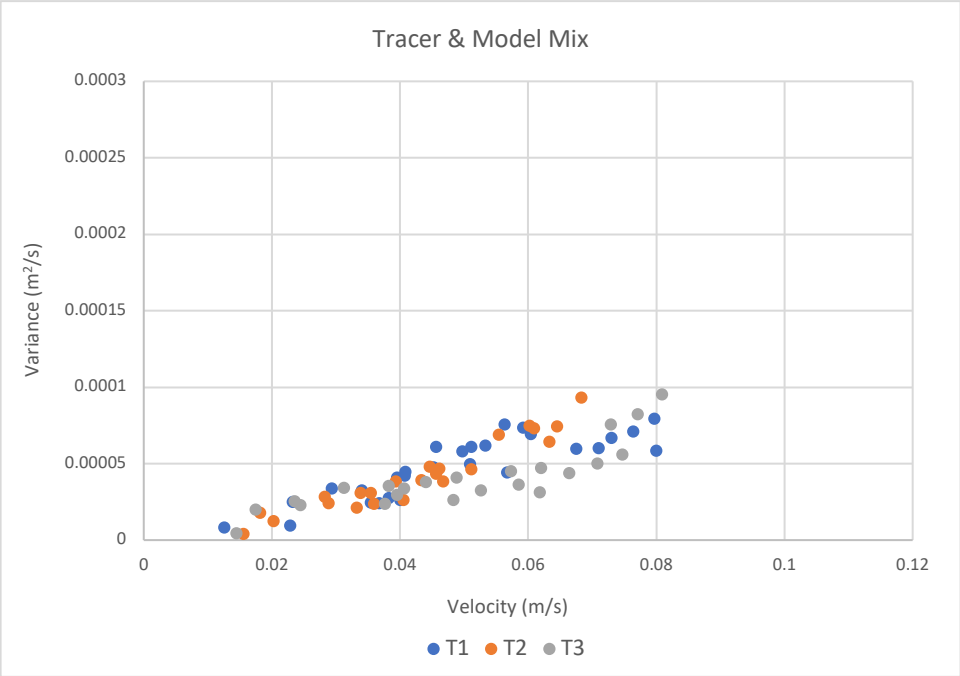

Figure 25. Variance of ADV velocity measurements in the x (streamwise) direction with corresponding average ADV velocities in the x direction for all observed flows in Trials 1-3 (T1-T3) in the Tracer & Model Mix incipient motion experiment.

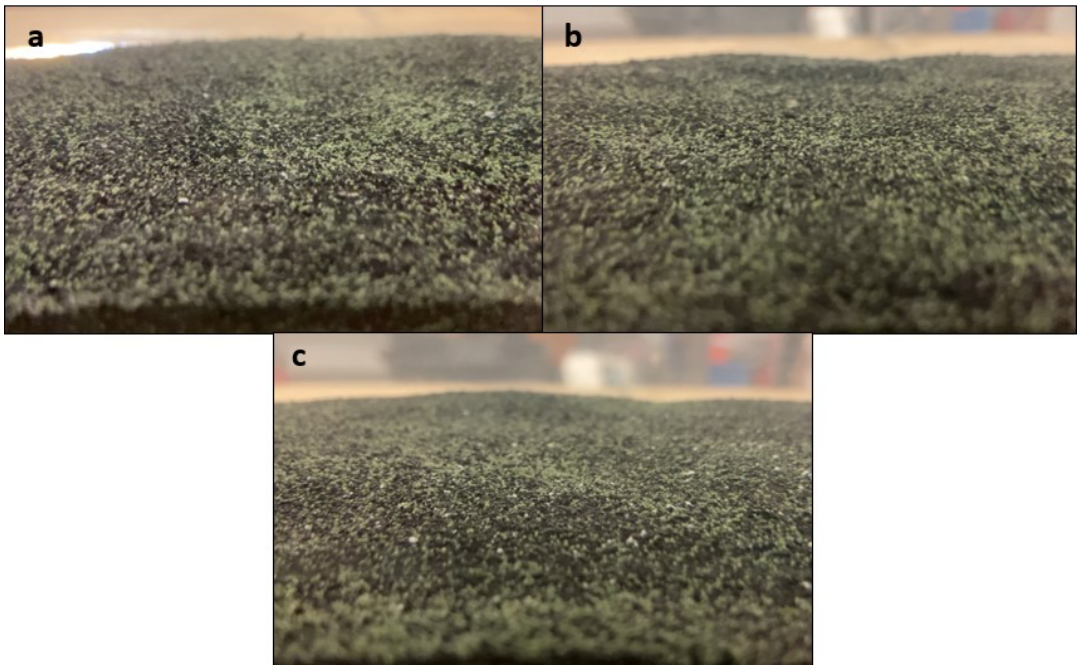

Figure 26. Close-up view of bed surface by ADV probe as seen in observational video recordings from Tracer & Model Mix incipient motion experiments. Photo a is from Trial 1, b from Trial 2, and c from Trial 3.

3.5.5. Incipient Motion Comparison

When the results from all four experiments are juxtaposed (Figure 27 and Figure 28), the trends for threshold of incipient motion are evident. The Model Full Range, Model D50, and Tracer & Model Mix experiments all depict incipient motion of model sediment occurring at around 0.06 m/s, right around the critical Shields threshold for motion (Figure 27), and at a bed shear stress in the range of 0.005 to 0.01 Pa (Figure 28). However, the Tracer D50 experiment depicts incipient motion of tracer particles occurring around 0.04-0.045 m/s at Shields parameters closer to 0.025, whereas the Tracer & Model Mix experiment depicts tracer sediment motion more in the range of 0.05-0.062 m/s and at Shields parameters hovering around the critical Shields threshold for motion (Figure 27). The bed shear stress required to move the tracer also increases slightly from about 0.005 Pa in the Tracer D50 experiment to 0.007 Pa in the Tracer & Model Mix experiment (Figure 28). The reasoning for this increase in velocity, Shields parameter, and bed shear stress to incite motion is likely the impact of "hiding effects". When a sediment mixture is more poorly sorted, as is the case with the Model Full Range and Tracer & Model Mix sediments, finer grains tend to nestle in between coarser grains, reducing their protrusion into the flow and somewhat crowding their mobility, requiring an increase in shear stress to move the finer grains (Einstein, 1950; Wiberg & Smith, 1987). It is also possible that the spherical tracer particles were caught in the angular pockets of the model sediment, further increasing the critical bed shear stress required for movement in the Tracer & Model Mix experiment when compared to the Tracer D50 experiment.

Also evident in Figure 27 and Figure 28 is that the Model Full Range experiment produced much more scatter in Shields parameters and bed shear stresses when compared to the Model D50 experiment. The higher amount of incipient motion observations below the critical Shields parameters for the Model Full Range experiment is likely partly due to the wider grain size

distribution (Table 6) of the model sediment when compared to the narrower distribution of the Model D50 experiment (Table 7). The wider grain size distribution introduces grains finer than 0.355mm as well as grains coarser than 0.500 mm, which may move at lower Shields parameters than grains strictly in the 0.355-0.500 mm range. However, the main reason for the increased scatter during the Model Full Range experiment is most likely the lower amount of turbulence that occurred during Trial 4, which could be due to the bed morphology, the pump performance, or both.

The Model D50 and Tracer D50 experiments results in Figure 27 and Figure 28 provide a direct comparison between the model and tracer sediment. On average, the tracer sediment moves at a velocity, Shields parameter, and bed shear stress of about 0.01 m/s, 0.01, and 0.004 Pa lower than the model sediment, respectively. Observations of incipient motion for the Model D50 experiment appear to line up better with the calculated critical Shields parameter than those for the Tracer D50, possibly meaning that the specific gravity of the moving tracer particles is slightly lower than the 1.05 of the model sediment. It is also possible that the sphericity of the tracer grains made it easier for particles to slip and slide across the bed surface, causing incipient motion to begin at lower Shields parameters than expected.

The Model Full Range and Tracer & Model Mix experiments display strikingly similar results (Figure 27 and Figure 28), with the key difference being that the tracer particles act as the spearheads for motion, with the model sediment following soon after in the Tracer & Model Mix experiment. There is less scatter present in the Tracer & Model Mix Shields parameters and bed shear stress data, which is likely what causes the average Shields parameter at the point of incipient motion (0.042) to be significantly higher than that of the Model Full Range experiment (0.034). It is important to note that a lot of the first model particles to move appeared to be coarser particles,

meaning particles ranging in the ~0.6-1.0 mm range, during both the Model Full Range and Tracer & Model Mix experiments. Normally, finer grains require less shear stress to initiate motion and are some of the first particles to begin to move, whereas coarser grains require more shear stress and move with increasing flows. However, as mentioned earlier, the difference in shear stress required to move coarse grains and finer grains decreases with more poorly-sorted mixtures, due to the "hiding effects" at the bed surface (Einstein, 1950; Wiberg & Smith, 1987). Often, coarser grains can actually move at a lower bed shear stress than what is needed to move finer grains, due to the relative protrusion of the coarser grains into the flow and the resultant increased drag acting on the particles that outweighs the relative gravitational forces holding the particles down (Wiberg & Smith, 1987).

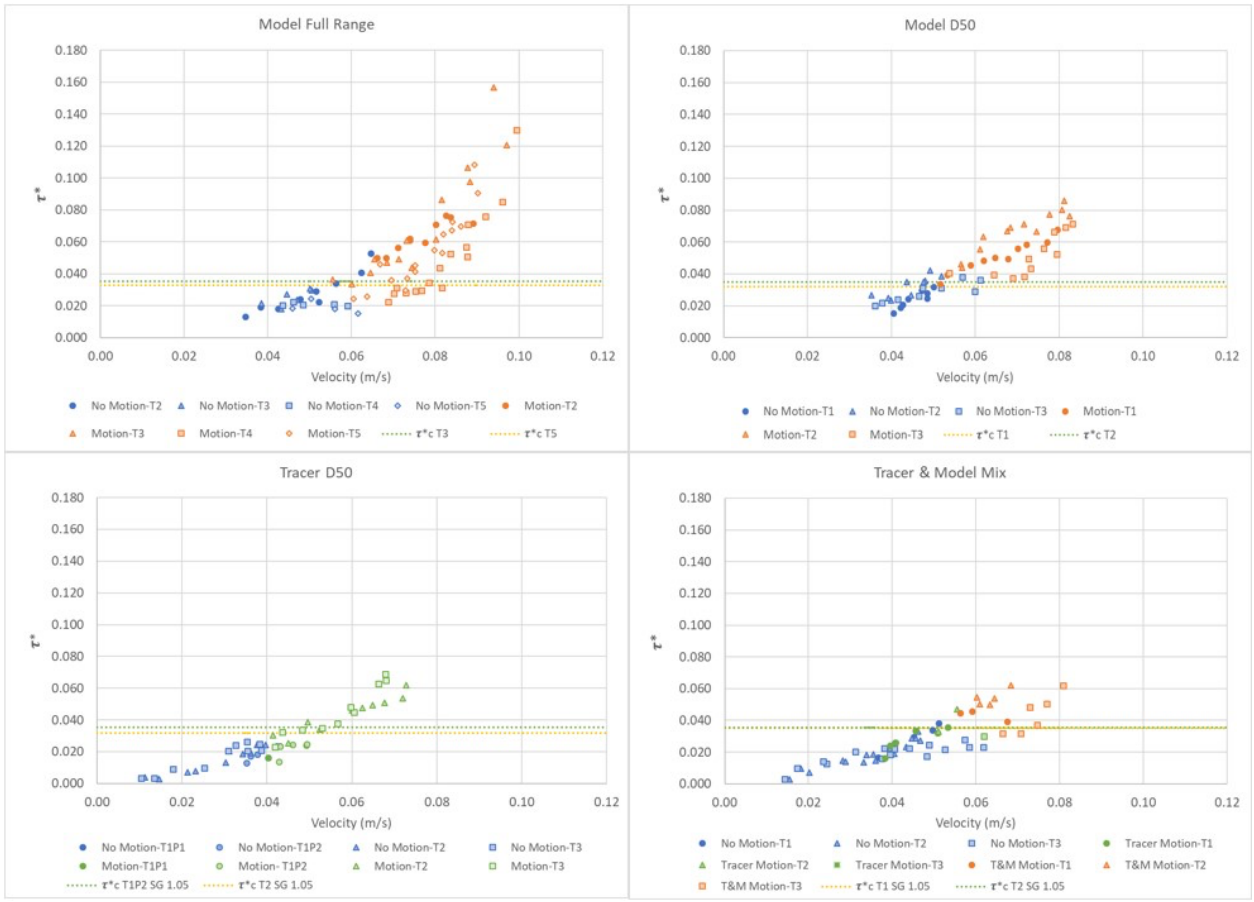

Figure 27. Average ADV x velocity of each ADV recording from all trials of all experiments and their respective calculated dimensionless Shields parameters, τ*, using a sediment specific gravity of 1.05. The blue shades represent no motion of particles observed during the majority of the recording, the green shades represent motion of tracer particles, and the orange shades represent motion of model sediment for the Model Full Range and Model D50 experiments, and motion of both tracer and model sediment particles for the Tracer & Model Mix. The dotted lines represent the upper and lower limits of calculated critical Shields thresholds for incipient motion, τ_c*.

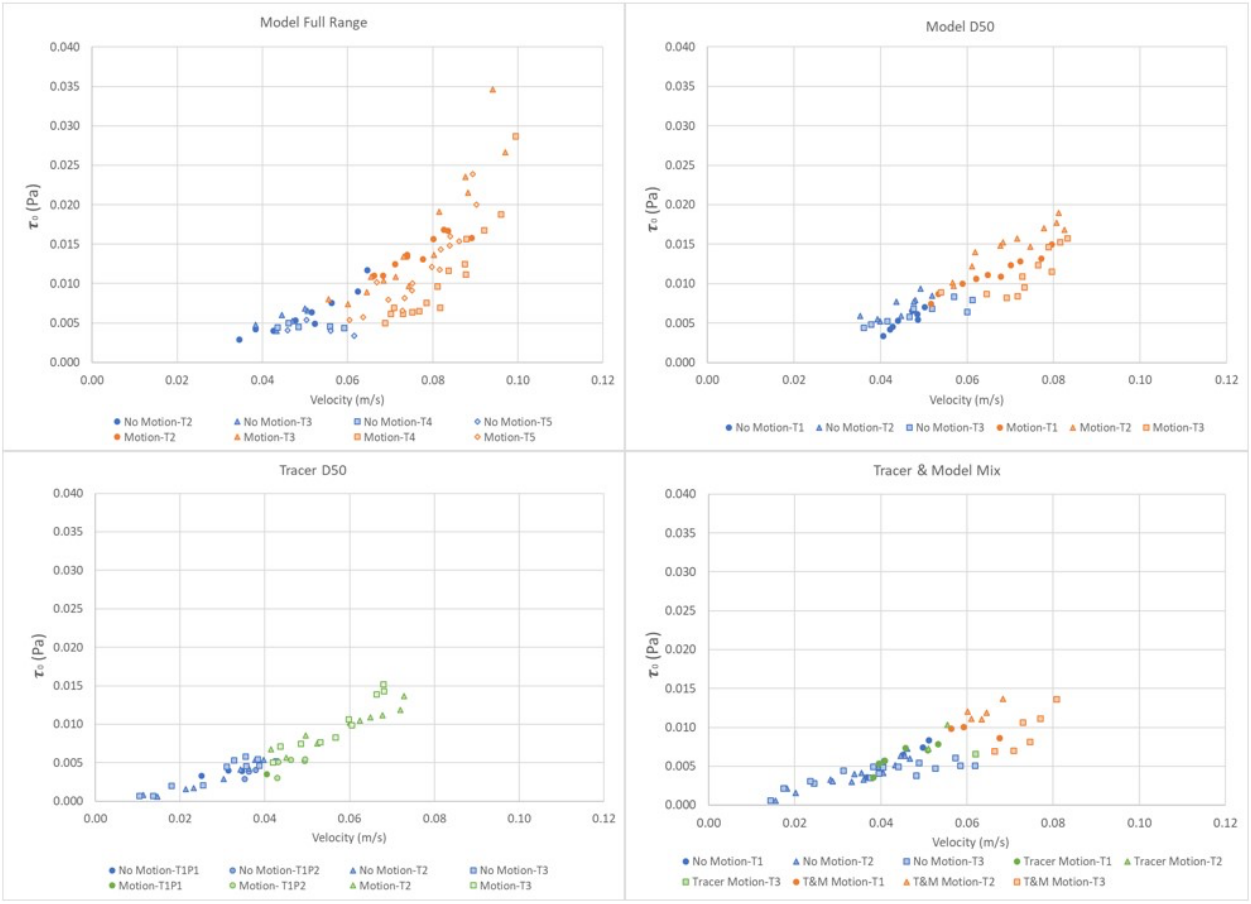

Figure 28. Average ADV x velocity of each ADV recording from all trials of all experiments and their respective calculated bed shear stresses, τ_0, in Pascals. The blue shades represent no motion of particles observed during the majority of the recording, the green shades represent motion of tracer particles, and the orange shades represent motion of model particles in the Model Full Range and Model D50 experiments and motion of both tracer and model sediment particles in the Tracer & Model Mix experiment.

The average velocities, Shields parameters, and bed shear stresses at the point of incipient motion for all four experiments are found in Table 10. It is important to note that these tabulated values are the averages of the first two recordings of each trial (during the gradual increase in pump voltage) in which particle motion was observed. Based on observational recordings, there were often several (i.e., more than two) recordings that could be considered incipient motion, as there was not always a linear increase in the quantity and constancy of particles moving as pump voltage and flows were increased. If all data where incipient motion was thought to be observed

was considered, the averages of the velocities, bed shear stresses, and Shields parameters would likely be slightly higher for all trials of all four experiments. However, to remain consistent, the first two recordings where incipient motion was first seen in each trial were the only recordings considered for these average values.

The average Shields parameters from Table 10 are plotted onto a Shields diagram to compare the observed critical Shields parameters for incipient motion to the average calculated critical Shields parameter for all experiments (Figure 29). Observational critical Shields values for all model sediments were at or above the calculated critical Shields parameter. Meanwhile, the observational critical Shields parameters for the tracer sediments remained below the calculated critical value, with tracer sediments from the Tracer D50 experiment presenting the lowest Shields values. Overall, when using the specific gravity of 1.05 for both the model and tracer sediments, the observation data line up well with the critical Shields thresholds calculated for each experiment. The results of these tests and calculations supply evidence for use of the *TKE* equation in flume environments with non-cohesive, lightweight, granular sediments.

Table 10. Average velocities, Shields parameters (τ^*), and bed shear stresses (τ_0) along with their standard deviations for all four experiments at their observed points of incipient motion. The Tracer & Model Mix data are differentiated by when incipient motion was first seen with tracer particles only, and then with both Tracer & Model particles together.

				Tracer & Model Mix	
Experiment	Model Full Range	Model D50	Tracer D50	Tracer	Tracer & Model
Average Velocity (m/s)	0.064	0.056	0.043	0.051	0.061
Velocity St. Dev (m/s)	0.005	0.003	0.000	0.010	0.004
Average $\boldsymbol{\tau}^*$	0.034	0.040	0.025	0.030	0.042
$\boldsymbol{\tau}^*$ St. Dev	0.010	0.003	0.004	0.008	0.008
Average $\boldsymbol{\tau}_0$ (Pa)	0.007	0.009	0.005	0.007	0.009
$\boldsymbol{\tau}_0$ St. Dev (Pa)	0.002	0.001	0.001	0.002	0.002

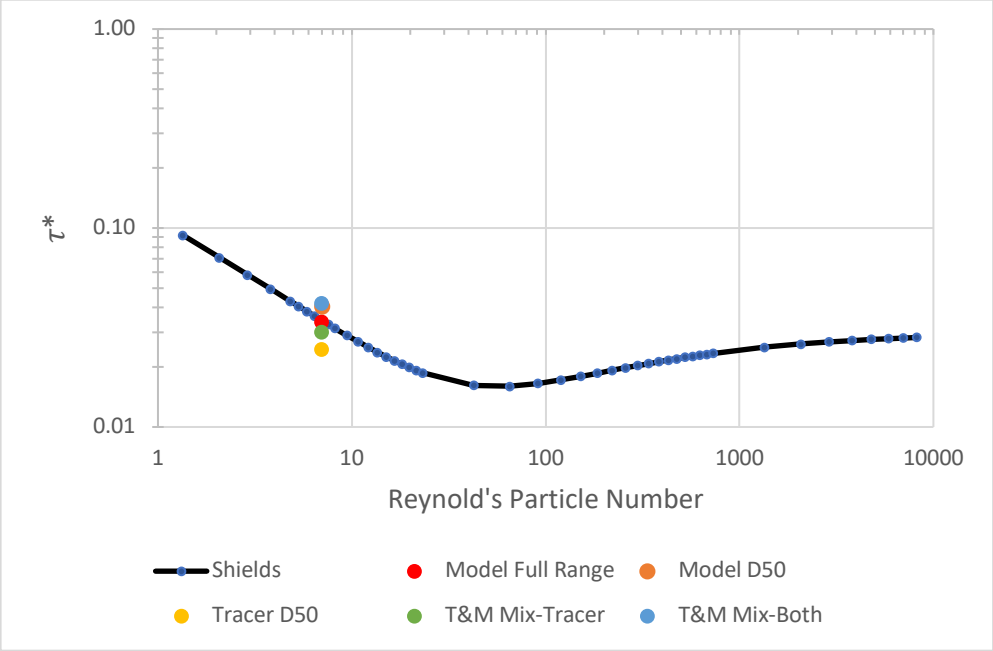

Figure 29. The average Shields parameter for all four experiments at the point of observed incipient motion, plotted on a Shields Diagram showing Reynold's Particle number at water temperature of 21.1° C with sediment SG 1.05 and varying sediment diameters from 0.15mm to 50mm versus the dimensionless Shields Parameter, τ*, representing critical tractive force for initiation of sediment motion.

3.5.6. Comparison with Other Bed Shear Stress Estimation Methods

To further corroborate the use of the *TKE* formula for estimating bed shear stress in these flume experiments, average velocities from the velocity profiles taken during the experiments are used to calculate bed shear stresses using both the law of the wall method and the Reynold's shear stress method. Both methods were tested and compared for Trial 1 of the Model D50 experiment at pump voltages of 6.7 and 6.9 (approximately 6.15 E-4 m^3/s or 9.75 GPM and 6.69 E-4 m^3/s or 10.6 GPM, respectively) and Trial 1 of the Tracer & Model Mix at a pump voltage of 7.1V (approximately 6.81 E-4 m^3/s, or 10.8 GPM).

The velocity profile and corresponding bed shear stresses at each probe height are seen in Figure 30 for Model D50 Trial 1 and Figure 31 for Tracer & Model Mix Trial 1. Following the

law of the wall method, the natural log of the distance above the bed is plotted with corresponding ADV velocities for both trials in Figure 32. The slope of the line fit to those data is then used to estimate shear velocity, u* (Eq. 2.20), which can then be used to estimate the average bed shear stress, τ_0 (Eq. 2.21) seen in Table 11 for both trials. The resultant bed shear stresses and Shields parameters from the Law of the Wall Method are about an order of magnitude greater than those of the *TKE* method, far surpassing the Shields critical threshold for motion of 0.035. The Law of the Wall method has been considered one of the least precise methods for estimating bed shear stress (Wilcock, 1996), so it is not surprising that it is not accurate here.

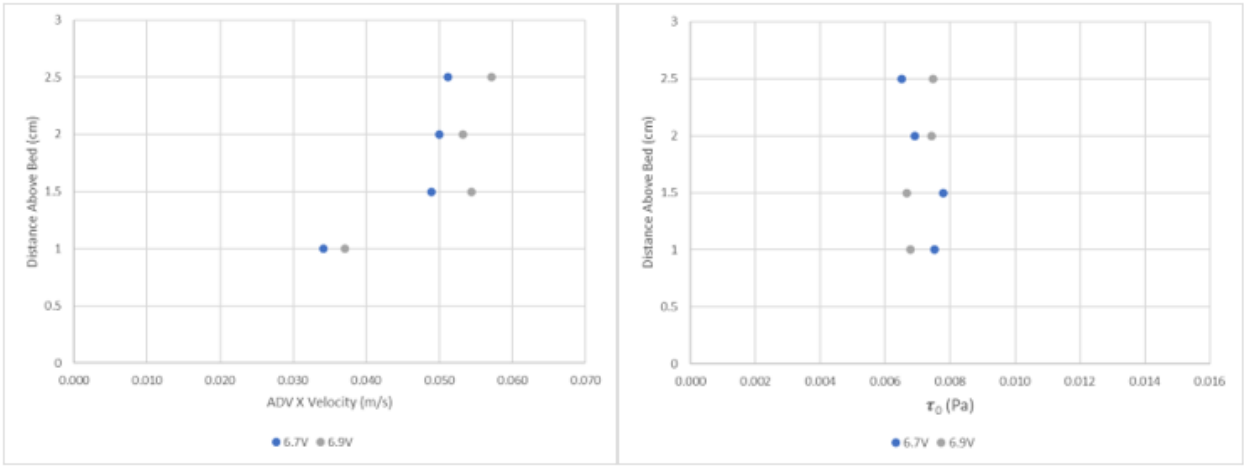

Figure 30. Velocity profile for Model D50 T1 at 6.7V and 6.9V on left and bed shear stress, τ_0, at corresponding distances from the bed surface on right.

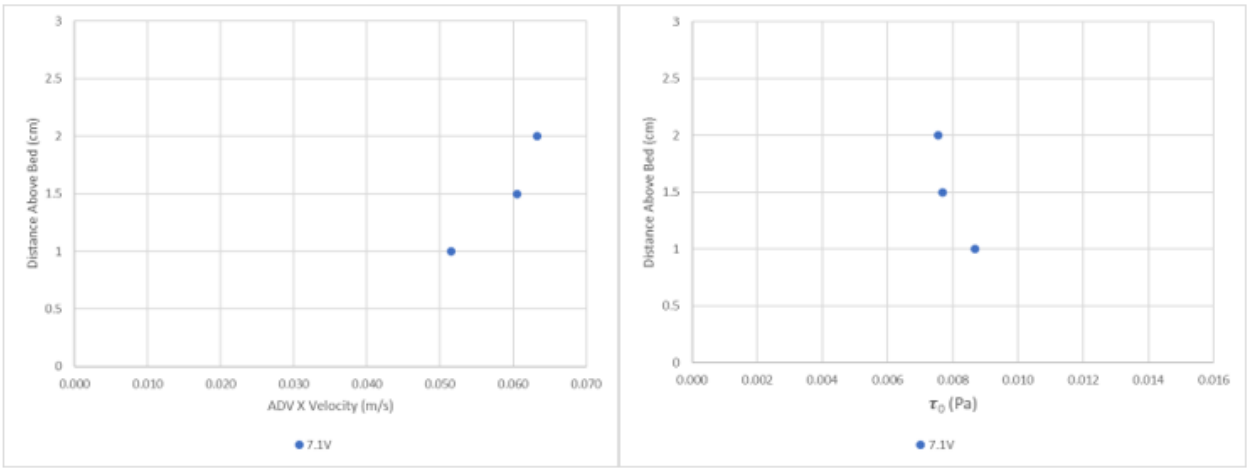

Figure 31. Velocity profile for Tracer & Model Mix T1 at 7.1V on left and bed shear stress, τ_0, at corresponding distances from the bed surface on right.

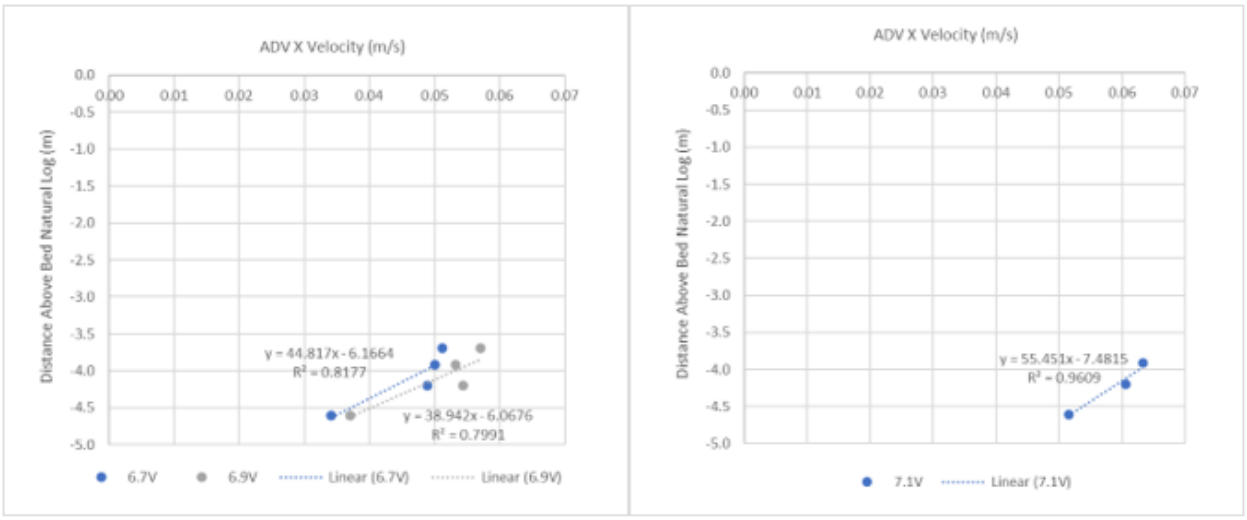

Figure 32. ADV X velocity with corresponding natural log of the distance from the bed for Model D50 T1 at 6.7V and 6.9V on left and Tracer & Model Mix T1 at 7.1V on right. Linear equations fit to data for use in calculating bed shear stress via Law of the Wall Method.

Table 11. Results from Law of the Wall method calculations for bed shear stress, $\boldsymbol{\tau_0}$, and resultant Shields parameters, $\boldsymbol{\tau^*}$, as compared to those calculated via the TKE method.

				Law of the Wall Method		TKE Method	
Experiment	Voltage	Distance Above Bed (cm)	ADV X Velocity (m/s)	$\boldsymbol{\tau_0}$ (Pa)	$\boldsymbol{\tau^*}$	$\boldsymbol{\tau_0}$ (Pa)	Avg $\boldsymbol{\tau^*}$
Model D50 T1	6.7 V	1	0.0342	0.0790	0.3579	0.0075	0.0325
		1.5	0.0489			0.0078	
		2	0.0500			0.0069	
		2.5	0.0512			0.0065	
	6.9 V	1	0.0371	0.1050	0.4757	0.0068	0.0321
		1.5	0.0545			0.0067	
		2	0.0533			0.0074	
		2.5	0.0571			0.0075	
Tracer & Model Mix	7.1V	1	0.0515	0.0519	0.2350	0.0087	0.0361
		1.5	0.0606			0.0077	
		2	0.0633			0.0075	

Calculated results using the Reynold's shear stress method (Eq. 2.22) are presented in Table 12. The bed shear stresses and resultant Shields parameters from the Reynold's shear stress method were very close to those from the *TKE* method; on average, the bed shear stresses and Shields parameters calculated via the TKE method were only about 11% higher than those of the Reynold's shear stress method. The TKE method produces results that are closer to the critical Shields parameter of 0.035, which is expected, as these velocity profiles were taken when the point of incipient motion was observed. However, the Reynold's shear stress method still produced relatively close values to those of the TKE Method, especially when compared to the Law of the Wall method. Nevertheless, results from both comparisons bolster the use of the TKE method for estimating bed shear stresses and Shields parameters in flume experiments with non-cohesive lightweight sediments.

Table 12. Results from Reynold's shear stress method calculations for bed shear stress, τ_0, and resultant Shields parameters, τ^*, as compared to those calculated via the TKE method.

Experiment	Voltage	Distance from Bed (cm)	Reynold's Method				TKE Method			
			τ_0 (Pa)	Avg. τ_0 (Pa)	τ^*	Avg. τ^*	τ_0 (Pa)	Avg. τ_0 (Pa)	τ^*	Avg. τ^*
Model D50 T1	6.7V	1	0.0065	0.0069	0.0292	0.0312	0.0075	0.0072	0.034	0.0325
		1.5	0.0095		0.0431		0.0078		0.0353	
		2	0.0051		0.0230		0.0069		0.0313	
		2.5	0.0065		0.0294		0.0065		0.0295	
	6.9V	1	0.0043	0.0062	0.0195	0.0280	0.0068	0.0071	0.0307	0.0321
		1.5	0.0045		0.0203		0.0067		0.0302	
		2	0.0090		0.0408		0.0074		0.0336	
		2.5	0.0070		0.0316		0.0075		0.0338	
Tracer & Model Mix T1	7.1V	1	0.0082	0.0067	0.0370	0.0302	0.0087	0.0080	0.0393	0.0361
		1.5	0.0071		0.0320		0.0077		0.0348	
		2	0.0048		0.0217		0.0075		0.0342	

3.6. Tracer Sediment Bar Seeding in LMRPM

Pictures were taken of the sand bars upstream of the Mid-Breton and Mid-Barataria sediment diversions before and after the tracer sediment was seeded into the bars (Figure 33). During the Y46 hydrograph run, several videos were taken at varying flows to follow the movement of the tracer. These videos show the tracer sediment becoming suspended, interacting with model sediment, entering the sediment diversions and depositing in the Mid-Breton and Mid-Barataria basins, or simply flowing downstream of the diversions and interacting with the sediment bed. After the Y46 hydrograph was run, pictures were taken of the sand bars upstream of the Mid-Breton and Mid-Barataria sediment diversions in both normal lighting and under UV lighting, to show how the tracer sediment had travelled by the end of the year (Figure 34). Video was also taken of the downstream reaches after the run, revealing how far the tracer had traveled.

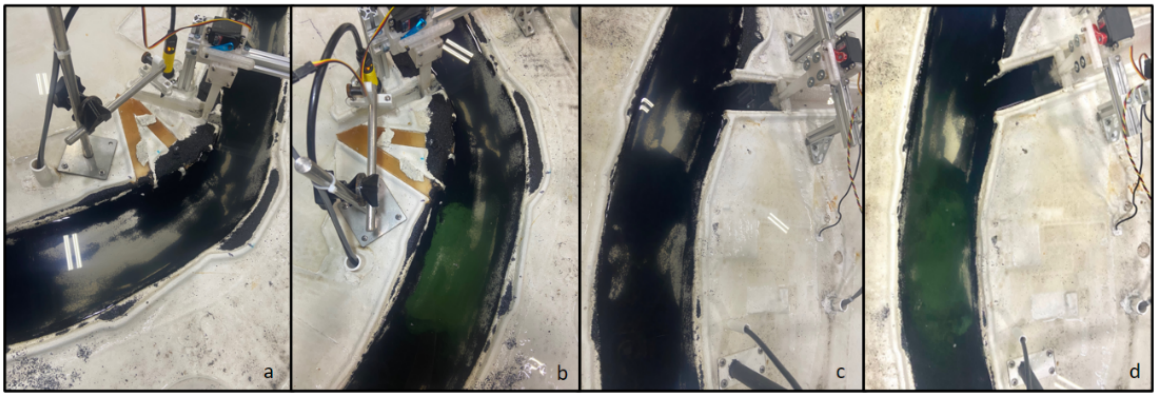

Figure 33. Sand bar upstream of Mid-Breton Sediment Diversion a) before tracer sediment added to bar and b) after tracer sediment added to bar. Sand bar upstream of Mid-Barataria Sediment Diversion c) before tracer sediment added to bar and d) after tracer sediment added to bar.

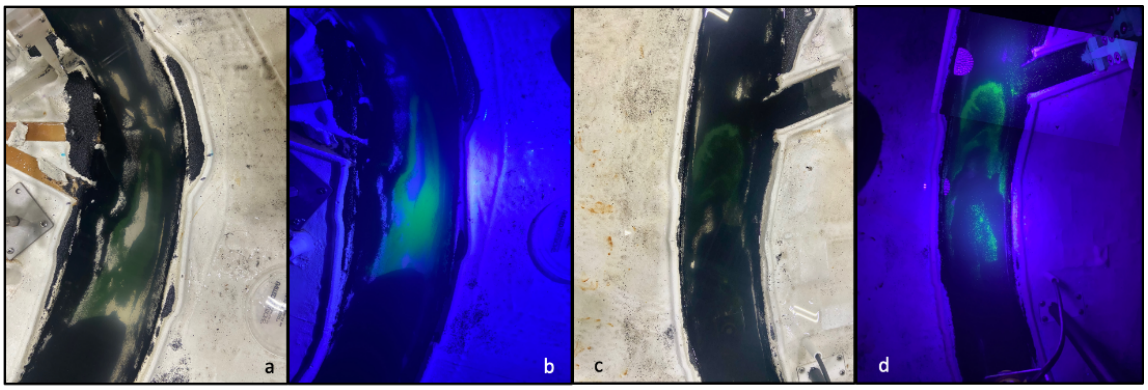

Figure 34. Sand bar upstream of Mid-Breton Sediment Diversion after hydrographic year was run on LMRPM a) under normal light and b) under UV light. Sand bar upstream of Mid-Barataria Sediment Diversion after hydrographic year was run on LMRPM c) under normal light and d) under UV light.

By the end of the hydrographic year, relatively small amounts of tracer particles had deposited in both the Mid-Breton and Mid-Barataria basins and had scattered all through the lower River into the Gulf of Mexico (~70+ model river miles). This is to be expected of typical LMRPM sediment during high flow years. Due to time constraints, the data available from this experiment were purely qualitative; no samples were taken to determine concentrations or grain sizes of tracer sediment in certain locations throughout the LMRPM. However, based on video evidence alone, the tracer sediment movement corresponded well with the model sediment movement, i.e., there was no specific observation of the tracer sediment moving without the model sediment moving as well.

Chapter 4. Discussion and Conclusion

At the LMRPM, a manufactured plastic sediment and altered sediment time scale are utilized to mimic, at a distorted horizontal: vertical scale, the unconsolidated sand transport in the prototype Lower Mississippi River. While the sediment dynamics of the Lower Mississippi River have been modeled rather accurately at the LMRPM despite a distorted scale, sediment dynamics upstream and downstream of sediment diversions and the similarities of the punctuated sediment transport between the model and prototype have not been explored in depth. By implementing a tracer sediment into the LMRPM that is discernible from the model sediment with UV light, sediment dynamics will not only be more easily observed at the particle level, but patterns in sediment deposition can be studied and quantified as well. For this reason, a fluorescent and magnetic tracer sediment with similar grain sizes and density to the model sediment was obtained. To ensure this tracer can be used in the LMRPM, testing of the sediment's properties such as its density, settling velocity, angle of repose, and Shield's parameter was conducted and compared to that of the model sediment.

The density of the tracer sediment was found to be 1.11 g/cm^3, which is about 6% higher than both the reported density of the particle and the density of the model sediment of 1.05 g/cm^3. However, this density may not be representative of all the tracer particles. Upon mixing the tracer sediment in water and a few milliliters of liquid detergent, 34% (by volume) of the particles floated at the water surface. To be able to use the tracer sediment for subsequent tests in this thesis, it was therefore required that all of the tracer sediment first be mixed with water, separated manually with a fine-mesh net, and then dried. A significant difference in color between sinking and floating particles prompted the idea that a lack of uniform fluorescent and magnetic coating of the particles led to the difference in particle density from what was specified by the manufacturer. Therefore,

it is possible that even the sinking tracer particles are not completely uniformly coated, and thus have a range of particle densities that averages out to be 1.11 g/cm^3.

The density difference between the tracer and model sediments is the key driver in the difference in settling velocities recorded for the different grain size classes. However, the model sediment's higher surface area due to its irregular shape causes the particles to experience more skin friction drag and pressure drag, along with more generalized instability as these forces cause the particles to rotate and vibrate as they settle, thereby slowing the settling velocity of the grains as well (Dey et al., 2019). These forces are more pronounced on irregularly shaped grains as compared to spherical grains of the same diameter (Dey et al., 2019). On average, the tracer particles settled at velocities twice those of the model sediment for all three grain size classes tested. All of the recorded settling velocities were in range with the calculated theoretical settling velocities from Stokes' equation (Eq. 2.13), whereas only the average observed settling velocity for the tracer 0.355-0.15 mm grains was slightly higher than the calculated theoretical velocity from Julien's equation (Eq 2.12). While it is possible that the differing densities could also impact the particles' angles of repose, the key driver of the model's 23.1° larger angle of repose is the model sediment's angular, shard-like grain shape. The tracer sediment is comprised of spherical grains, with the occasional cluster of spherical grains glued together by their coating. The sphericity of these grains makes them much more likely to slide and become dislodged from other particles, leading to slope failure at a lower slope angle than might be experienced by the model sediment with its angular, interlocking grains.

Incipient motion tests in the hydraulic flume revealed consistent results for model sediment incipient motion thresholds in all three experiments where model sediment was involved (Model Full Range, Model D50, Tracer & Model Mix). On average, incipient motion of model sediment

began at velocities of 0.056-0.064 m/s, Shields parameters of 0.034-0.042, and bed shear stresses of 0.007 to 0.009 Pa. Tracer particles began to move at average velocities around 0.043-0.051 m/s, Shields parameters of 0.025-0.030, and bed shear stresses of 0.005-0.007 Pa. The higher velocities, Shields parameters, and bed shear stresses of the tracer occurred during the Tracer & Model Mix experiment, suggesting that the forces required to move the tracer sediment were higher when the tracer sediment was forced to overcome the "hiding effects" that finer grains face when mixed with coarser grains. While significant scatter is to be expected in tests with turbulent flow, all four experiments presented consistent observational and numerical data, despite this turbulence-induced variability. Of particular importance is that the Tracer & Model Mix results compare very well with the Model Full Range results, where motion of model particles began at velocities around 0.064 m/s, Shields parameters of 0.034, and bed shear stresses of 0.007 Pa. For the Tracer & Model Mix experiment, motion of model particles began at velocities around 0.061 m/s, Shields parameters of 0.042, and bed shear stresses of 0.009 Pa, with tracer motion beginning slightly before model motion (velocity of 0.051 m/s, Shields 0.03, bed shear stress 0.007 Pa). This suggests that when the tracer sediment replaces the D50 grain sizes of the model sediment's typical grain size distribution, incipient motion of particles begins at a very similar velocity, Shields parameter, and bed shear stress to that of the LMRPM model sediment.

As was noted by Kramer (1935) and Mofjeld & Lavelle (1987), observational analysis of incipient motion is extremely difficult and highly subjective, as there are often many different observations that could fit into the "no motion" or "motion" category. While the requirement was that a few particles roll, slide, or saltate at the bed surface for the majority of the observational recording, particles were not timed and their motion was subjectively gauged as insufficient or sufficient in order to be considered "incipient" by the viewer. While the classifications of

observations at times felt variable, the plotted results revealed fairly distinct trends between “no motion” and “motion”, and observed incipient motion tended to hover closely around the calculated critical Shields parameters for all four experiments.

While the tracer sediment’s settling velocities and angles of repose are significantly different from those of the model sediment, flume tests proved the threshold for incipient motion to be similar to that of the model sediment. And, when the tracer and model sediment is mixed together, incipient motion of particles occurs at thresholds sufficiently similar to that of the typical model sediment. Qualitative results from the bar-seeding experiment further corroborated the flume results, providing support for the tracer sediment’s implementation in the LMRPM.

4.1. Future Work

Future flume experiments with the sediment mixtures used in this study should focus on comparisons of dune formation, propagation, and morphology. Dune characteristics are impacted by all the parameters tested in this study. While the thresholds for motion between the tracer and model sediment may be deemed as sufficiently similar to allow for tracer implementation in the LMRPM, the similarities between dune formations and translations are unknown. On its own, the tracer sediment may not be able to reproduce the same dune characteristics observed in the model sediment. However, when mixed with the model sediment, the tracer sediments could possibly nestle amongst the more angular model sediments, maintaining the typical dune heights that the model sediment displays.

In future incipient motion experiments, it would be advantageous to focus more on transport rates of sediments instead of thresholds for motion. There is no standard definition for what constitutes incipient motion and observational analysis is highly subjective, so it is difficult to produce results that can be universally significant. While these experiments were useful to directly

compare two types of sediment, a study employing quantitative calculations of sediment transport could provide more standardized results for use in comparison (Lavelle & Mofjeld, 1987).

The preliminary bar-seeding experiment in the LMRPM provided a first glimpse of the intricacies of injecting the tracer sediment into the model and adequately recording its movement. To capture good videos of the tracer movement, it is recommended to set up several UV lights on highly adjustable rigs all throughout the specific segment of the model being studied. For example, if studying the sediment movement from the upstream bar of the Mid-Breton sediment diversion, it is recommended to have a UV light set up at every river mile to ensure that the tracer is adequately illuminated in videos. A long-armed, highly adjustable camera stand is recommended to allow for steady, yet mobile capture of tracer sediment motion as it traverses several river miles. It is also recommended that one specific location be studied at a time, unless there are multiple cameras set up at different locations to record simultaneously.

Depending on the type of data desired from usage of the tracer sediment, different mixtures of the tracer are suggested. If wanting more qualitative results, such as tracking sediment movement, just the tracer sediment of a specific grain size can be seeded or injected in desired locations. If more quantitative data, such as grain size distributions and tracer concentrations in specific locations are desired, it is recommended to first mix the tracer sediment with model sediment, with the tracer sediment replacing a specific grain size class of the model sediment. In this way, the tracer and model sediment mixture will behave more similar to the Model Full Range sediment, and data will be more representative of the typical sediment transport that occurs on the LMRPM. Furthermore, depending on the specific location where the tracer mixture is injected in the model, the grain size fraction that the tracer replaces should be altered, as grain size distributions show significant fining from upstream to downstream locations.

This study and tracer sediment could prove useful for further research into sediment dynamics in and around diversions, with specific focus on point bar dynamics. Methods such as seeding point bars or other bed forms with tracer sediment could shed light on sediment capture efficiency of diversions. Injecting the sediment tracer into the LMRPM once every 10 years would reveal how certain grain size fractions of sediment interact with sediment diversions; how far these grain sizes can travel in one or subsequent years; how much, where, and why they might accumulate in certain locations, and how accurately the model's sediment transport mimics the punctuated transport present in the prototype. A 50-Year experiment on the LMRPM with projected sea level rise and tracer implementation will also reveal how much of the tracer has been incorporated deeper into the channel bed, and how much the increased backwater effects have slowed its propagation downstream. While this experiment is centered on a broader understanding of the aforementioned dynamics, many new research questions and studies could build upon it. On a broader scope, this and other studies on sediment transport dynamics in the LMRPM are beneficial to agencies such as the CPRA and The Water Institute of the Gulf in terms of their own modeling and real-world plans for Mississippi River sediment-related projects.

References

Agudo, J., Illigmann, C., Luzi, G., Laukart, A., Delgado, A., & Wierschem, A. (2017). Shear-induced incipient motion of a single sphere on uniform substrates at low particle Reynolds numbers. *Journal of Fluid Mechanics*, *825*, 284-314.

Al-Hashemi, H. M. B., & Al-Amoudi, O. S. B. (2018). A review on the angle of repose of granular materials. *Powder technology*, *330*, 397-417.

Allison, M. A., Yuill, B. T., Meselhe, E. A., Marsh, J. K., Kolker, A. S., & Ameen, A. D. (2017). Observational and numerical particle tracking to examine sediment dynamics in a Mississippi River delta diversion. *Estuarine, Coastal and Shelf Science*, *194*, 97-108.

BCG Engineering & Consulting, I. (2015). *Proof of concept report on tests of instrumentation, automation, and hydraulics in a distorted scale physical model of a reach of the Mississippi River*.

Buffington, J. M., & Montgomery, D. R. (1997). A systematic analysis of eight decades of incipient motion studies, with special reference to gravel-bedded rivers. *Water Resources Research*, *33*, 1993 - 2029.

CPRA. (2019). Lower Mississippi River Physical Model: Operations & Management Manual.

Dey, S., Ali, S. Z., & Padhi, E. (2019). Terminal fall velocity: the legacy of Stokes from the perspective of fluvial hydraulics. *Proceedings of the Royal Society A*, *475*(2228), 20190277.

Dingman, S. L. (2009). *Fluvial hydraulics*. oxford university press.

Einstein, H. A. (1950). *The bed-load function for sediment transportation in open channel flows*. US Department of Agriculture.

Goring, D. G., & Nikora, V. I. (2002). Despiking acoustic Doppler velocimeter data. *Journal of Hydraulic Engineering*, *128*(1), 117-126.

Grass, A. J. (1970). Initial instability of fine bed sand. *Journal of the Hydraulics Division*, *96*(3), 619-632.

Ho, J., Coonrod, J., Gill, T., & Mefford, B. (2010). Case study: movable bed model scaling for bed load sediment exclusion at intake structure on Rio Grande. *Journal of Hydraulic Engineering*, *136*(4), 247-250.

Hooper, M. (2019). *Quantitative Evaluation of a Lightweight Sediment for a Physical Model of the Lower Mississippi River* Louisiana State University and Agricultural & Mechanical College].

Julien, P., & Tuzson, J. (2003). River Mechanics. *Appl. Mech. Rev.*, *56*(2), B30-B31.

Kármán, T. (1930). Mechanische änlichkeit und turbulenz. *Nachrichten von der Gesellschaft der Wissenschaften zu Göttingen, Mathematisch-Physikalische Klasse*, *1930*, 58-76.

Kleinhans, M. G., Leuven, J. R., Braat, L., & Baar, A. (2017). Scour holes and ripples occur below the hydraulic smooth to rough transition of movable beds. *Sedimentology*, *64*(5), 1381-1401.

Kramer, H. (1935). Sand mixtures and sand movement in fluvial model. *Transactions of the American Society of Civil Engineers*, *100*(1), 798-838.

Lavelle, J. W., & Mofjeld, H. O. (1987). Do Critical Stresses for Incipient Motion and Erosion Really Exist? *Journal of Hydraulic Engineering*, *113*(3), 370-385. https://doi.org/doi:10.1061/(ASCE)0733-9429(1987)113:3(370)

Mori, N., Suzuki, T., & Kakuno, S. (2007). Noise of acoustic Doppler velocimeter data in bubbly flows. *Journal of engineering mechanics*, *133*(1), 122-125.

Nittrouer, J. A., Mohrig, D., & Allison, M. (2011). Punctuated sand transport in the lowermost Mississippi River. *Journal of Geophysical Research-Earth Surface*, *116*. https://doi.org/Artn F0402510.1029/2011jf002026

Parker, G., Toro-Escobar, C. M., Ramey, M., & Beck, S. (2003). Effect of floodwater extraction on mountain stream morphology. *Journal of Hydraulic Engineering*, *129*(11), 885-895.

Pope, N., Widdows, J., & Brinsley, M. (2006). Estimation of bed shear stress using the turbulent kinetic energy approach—A comparison of annular flume and field data. *Continental Shelf Research*, *26*(8), 959-970.

Pugh, C. A., & Dodge, R. A. (1991). DESIGN OF SEDIMENT NODELS. *STREAM MODELING*, 61.

Shields, A. (1936). Anwendung der Aehnlichkeitsmechanik und der Turbulenzforschung auf die Geschiebebewegung. *PhD Thesis Technical University Berlin*.

Sontek. (2001). Sontek/ysi advfield/hydra acoustic doppler velocimeter (field) In.

Soulsby, R. L. (1983). The bottom boundary layer of shelf seas. In *Elsevier oceanography series* (Vol. 35, pp. 189-266). Elsevier.

Stapleton, K., & Huntley, D. (1995). Seabed stress determinations using the inertial dissipation method and the turbulent kinetic energy method. *Earth surface processes and landforms*, *20*(9), 807-815.

Stokes, G. G. (1901). *Mathematical and physical papers* (Vol. 3).

Traphagan, J. (2023). MATLAB Loop Structure. In. Louisiana State University.

Vanoni, V. A. (1964). Measurements of critical shear stress for entraining fine sediments in a boundary layer.

Vanoni, V. A., Benedict, P. C., Bondurant, D. C., McKee, J. E., Piest, R. F., & Smallshaw, J. (1966). Sediment transportation mechanics: Initiation of motion. *Journal of the Hydraulics Division*, *92*(2), 291-314.

Vollmer, S., & Kleinhans, M. G. (2007). Predicting incipient motion, including the effect of turbulent pressure fluctuations in the bed. *Water Resources Research*, *43*(5).

Wiberg, P. L., & Smith, J. D. (1987). Calculations of the critical shear stress for motion of uniform and heterogeneous sediments. *Water Resources Research*, *23*(8), 1471-1480.

Yuill, B. T., Gaweesh, A., Allison, M. A., & Meselhe, E. A. (2016). Morphodynamic evolution of a lower Mississippi River channel bar after sand mining. *Earth surface processes and landforms*, *41*(4), 526-542.

Vita

Julia Mudd is from Easton, Massachusetts. She studied a double major in Environmental Earth Science and Spanish at Tulane University, achieving her Bachelors of Science in May, 2017. After working in New Orleans for a year, and then working and backpacking through South and Central America for another year, Julia applied to the LSU Civil and Environmental Engineering Masters program. In January 2020, she was awarded a graduate research assistantship at the LSU Center for River Studies under the advisory of Dr. Clinton Willson. Julia hopes to achieve her Masters in Civil Engineering-Water Resources Engineering in August 2023.